Computational Modeling of Forearm Rotation

Tran Viet Nam
A0243474A

Advisor: Professor Leow Wee Kheng
Department of Computer Science
School of Computing
National University of Singapore

Ph.D. Qualifying Examination
Research Paper
October 17, 2022

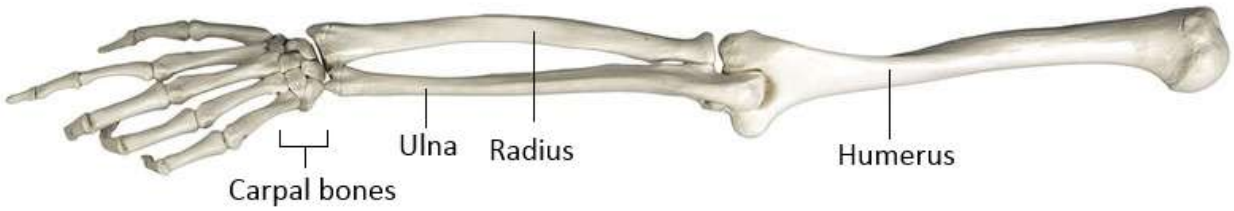

Figure 1: Anatomy of the arm. The humerus is the upper arm, the ulna and the radius form the forearm, and the carpal bones are the wrist bones.

Abstract

The forearm allows humans to move and manipulate objects. It is susceptible to injuries and degeneration over time. A wide range of forearm injuries require surgical treatment, which is a complex procedure. If a surgical operation is not performed appropriately, it can result in pain and significant loss of forearm functionality. Given the complexity of forearm surgery, in order to ensure a successful procedure, pre-operative planning is vital. Computational modeling of forearm rotation is a major approach of pre-operative planning. Existing works on modeling forearm motion mostly focus on research uses and are not feasible for routine clinical application. The overall goal of this research is to provide a solution to this problem by constructing a subject-specific, straightforward and clinically useful forearm model that facilitates routine pre-operative planning. This QE paper presents the findings of initial research on modeling the motion of forearm bones in a manner that facilitates routine clinical applications.

1 Introduction

The forearm allows humans to move and manipulate objects. It is susceptible to injuries and degeneration over time, which limits its normal functionality. These injuries are often caused by overuse, accidental impacts or old age. For a wide range of forearm injuries, surgery is necessary to repair the damage.

Forearm surgery is a complex procedure. For example, the surgical treatment for Essex-Lopresti lesion, which is a combination of elbow bone fracture, wrist joint disruption and forearm soft tissue rupture, remains an open problem [1]. Currently, the surgery often involves replacement and reconstruction of forearm bone and soft tissues [2, 3]. It requires the surgeon to determine the optimal implant diameter for the replaced bone as well as the location of the graft for the reconstructed soft tissues. If these repair parameters are not accurately determined, the procedure may be ineffective, resulting in pain and significant loss of forearm functionality. Given the complexity of forearm surgery, in order to ensure a successful procedure, precise pre-operative planning is vital.

Computational modeling is a major approach of pre-operative planning. It has to model forearm functionality accurately. To this end, the model must be able to describe 3D geometries of forearm bones and soft tissues as well as their interactions during forearm motion. Since the interactions are complex and subject-specific, modeling forearm functionality re-

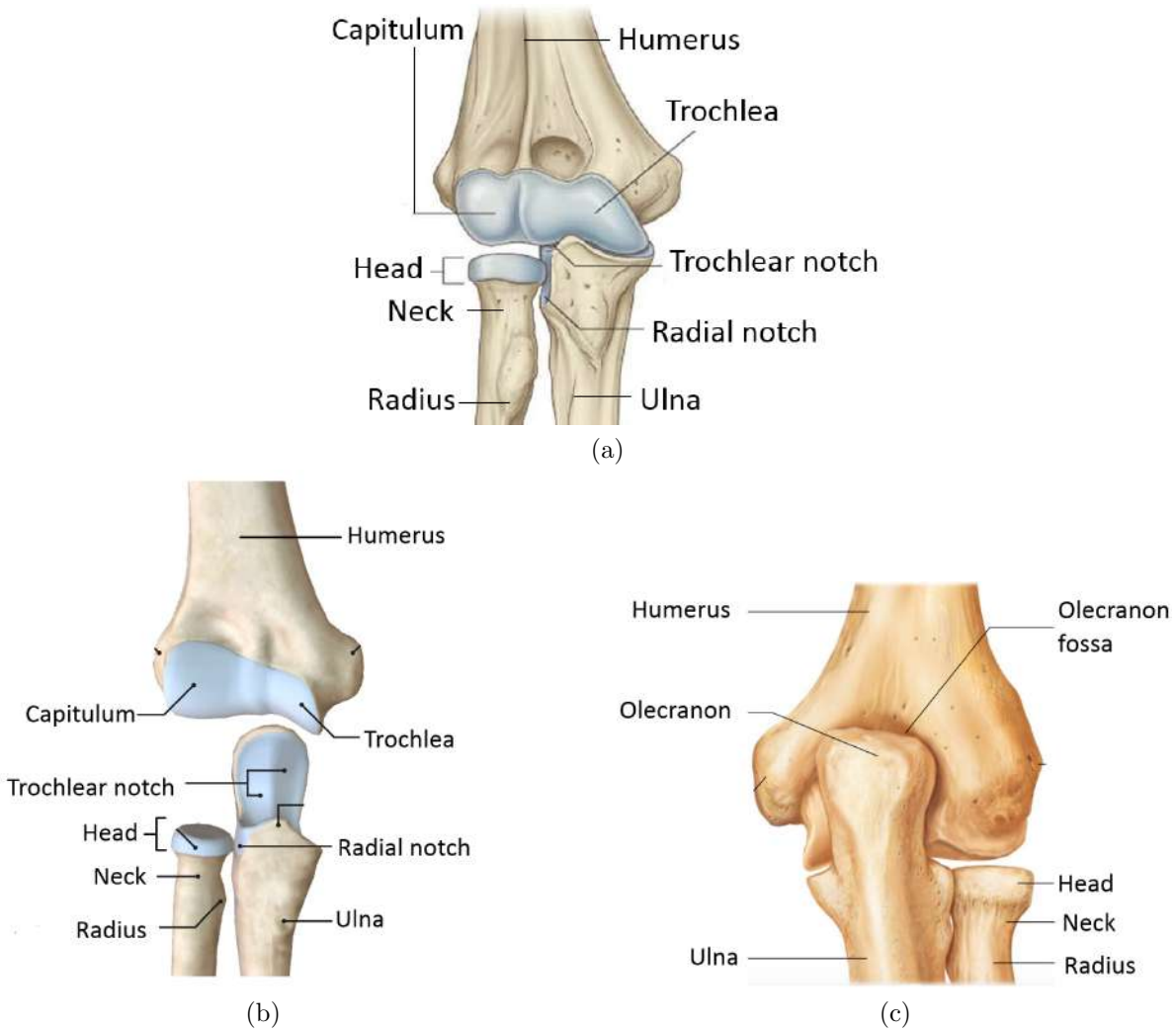

Figure 2: Anatomy of the elbow. (a) Anterior (frontal) view of elbow joint. (b) Separate bones of elbow joint. (c) Posterior (rear) view of elbow joint.

mains difficult.

Existing works on modeling forearm motion can be categorized as abstract models, static models, kinematic models and dynamic models. Abstract models describe joints as points and bones as straight lines connecting the points. They are frequently used for computer animation. Since they do not model 3D geometries and interactions of the bones and soft tissues, they are omitted from this discussion. Static models [4, 5, 6, 7, 8, 9, 10, 11, 12, 13, 14, 15, 16, 17, 18, 19] model forearm bones as a sequence of geometrical models at discrete poses. Methods using static models use a subject's computer tomography (CT) or 4D computer tomography (4DCT) scans to obtain a sequence of discrete 3D poses. Although they are subject-specific, straightforward to develop and can model soft tissues, they cannot model continuous bone motion.

Kinematic models [7, 11, 20, 21, 22, 23, 24] model forearm bones as a continuous sequence of geometrical models over a range of motion, in the absence of forces. Methods using kine-

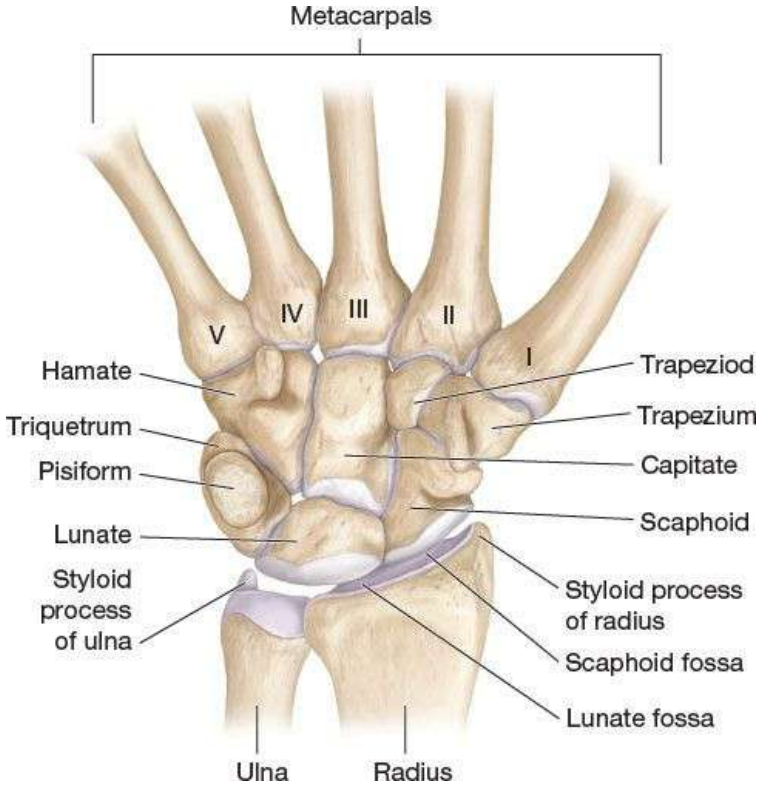

Figure 3: Anatomy of the wrist.

matic models construct a geometrical model from a CT or 3D rotational x-ray (3DRX) scan. They then use motion data captured using various techniques such fluoroscopy, 4DCT, 4D rotational x-ray (4DRX) or motion capture (mocap) to determine forearm bone poses during motion. Dynamic models [25, 26, 27, 28, 29, 30] model both bone motion and forces involved. A basic dynamic model includes a muscle model and a musculoskeletal model that describe joint forces. They apply forward dynamics and 3D model alignment to obtain 3D bone poses during motion. Since kinematic and dynamic models involve complex computations such as forward kinematics and forward dynamics, both models are too sophisticated for routine clinical use. They are more appropriate for medical research.

The overall research objective is to develop a forearm model that describes the motion and interactions of bones and soft tissues for routine clinical applications. As a start, this QE paper focuses on developing a computational model that includes the forearm bones, the wrist bones and part of the upper arm bone, and just a selected set of soft tissues. Using only one CT scan, which is routinely captured for surgery patients, the model is expected to be straightforward and useful for routine clinical applications.

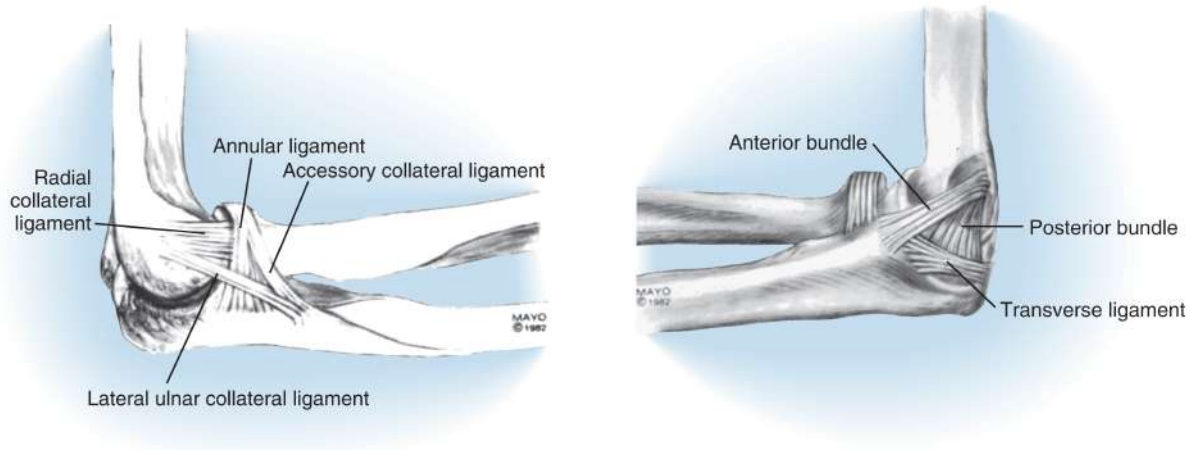

(a) (b)

Figure 4: Main elbow ligaments [31]. (a) Lateral collateral ligament (LCL) complex. (b) Medial collateral ligament (MCL) complex.

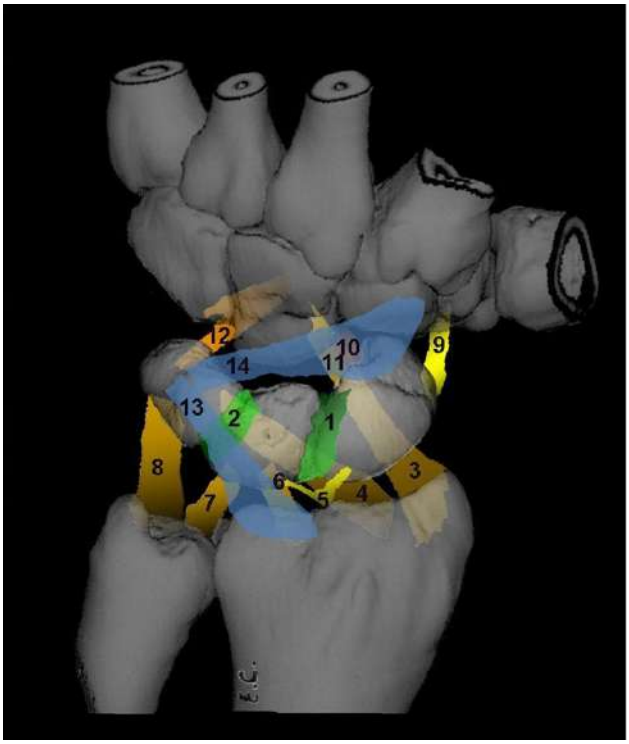

Figure 5: Main wrist ligaments [32].

2 Forearm Functional Anatomy

2.1 Anatomy of the Arm

The arm consists of three long bones, namely the humerus, radius and ulna, and several small bones that make up the palm and the fingers (Fig. 1) [31]. The radius and the ulna

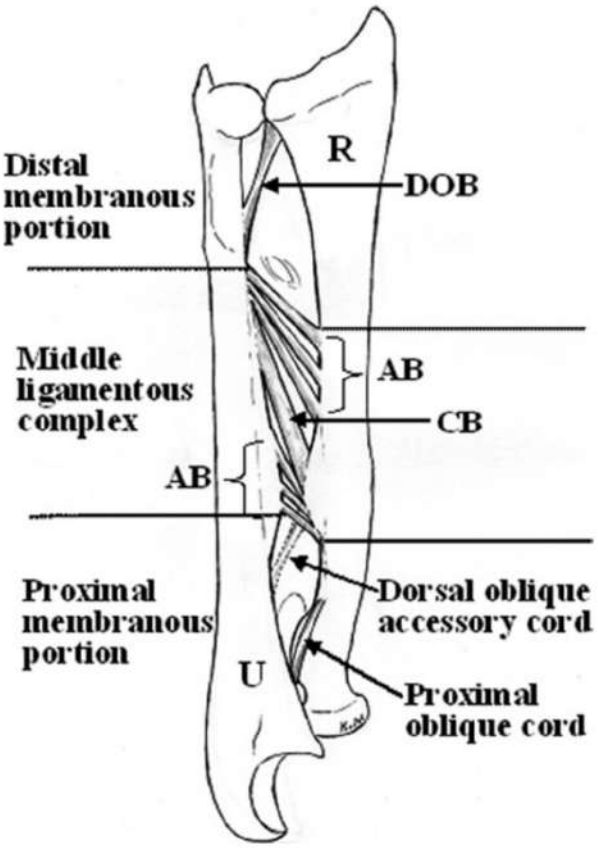

Figure 6: Interosseous membrane (IOM) [4]. The proximal portion contains the dorsal oblique accessory cord (DOAC) and the proximal oblique cord (POC). The middle portion houses both the accessory band (AB) and the central band (CB). The distal portion contains the distal oblique bundle (DOB).

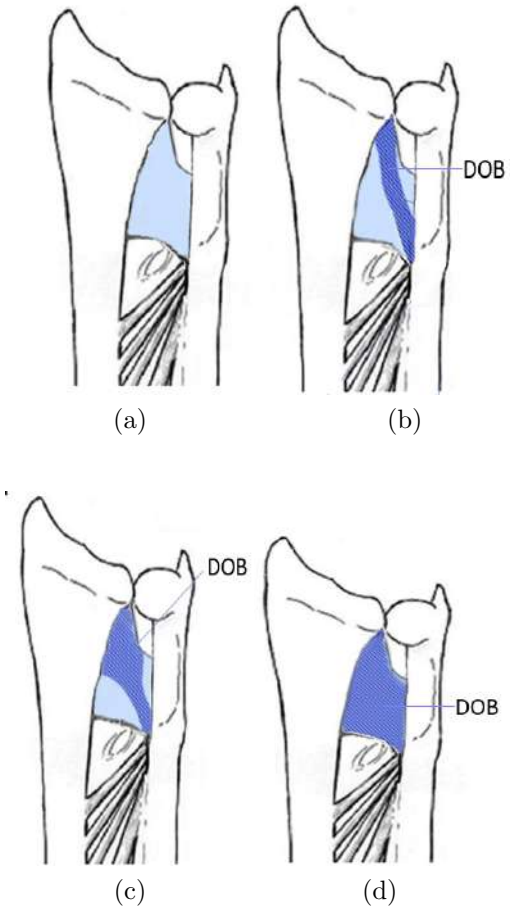

Figure 7: Anatomical variation of the IOM's distal portion [33]. (a) Some forearms do not have the DOB. (b, c, d) For forearms that have the DOB, the DOB can vary in shape.

form the forearm, and the humerus is the upper arm. The forearm is connected to the humerus at the elbow joint and to the palm at the wrist joint. The elbow consists of three joints (Fig. 2). The humeroulnar joint is a joint between the trochlea on the humerus and the trochlear notch of the ulna. The humeroradial joint is a joint between the capitulum on the humerus and the head of the radius. The proximal radioulnar joint (PRUJ) is made up of the head of the radius and the radial notch of the ulna. The wrist consists of two joints (Fig. 3). The radiocarpal joint is made up of the radius and the carpal bones of the wrist. The ulna is not part of the wrist joint, although it moves together with the radius. The distal radioulnar joint (DRUJ) is made up of the distal parts of the radius and the ulnar. The humerus is joined to the shoulder at the shoulder joint, which is a ball-and-socket joint.

The forearm also consists of soft tissues such as cartilages and ligaments [37]. Cartilage is a firm and flexible tissue at the articulating surface of a joint. It protects the joint from

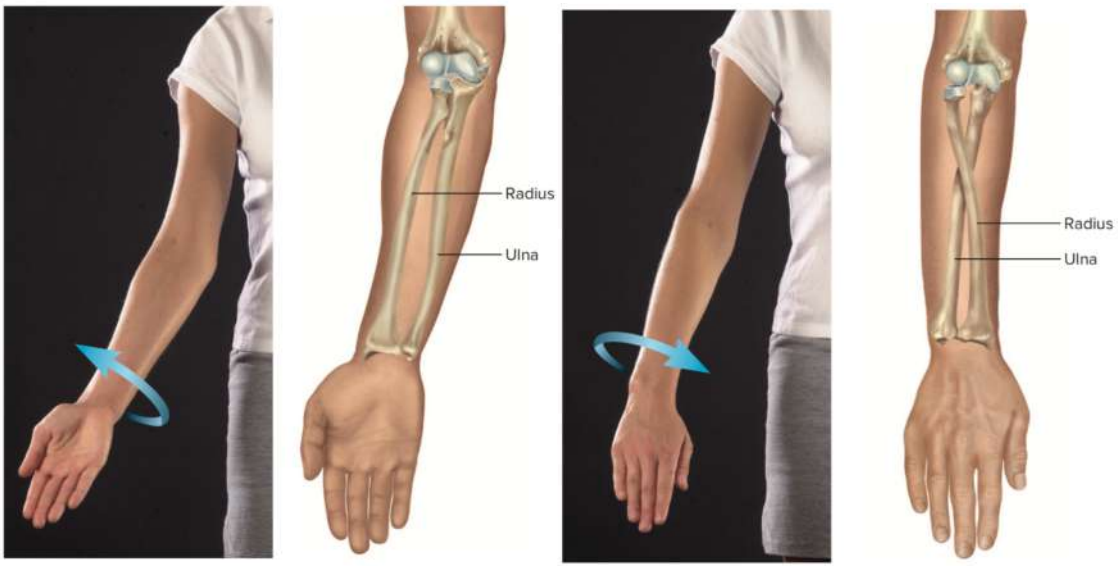

(a) (b)

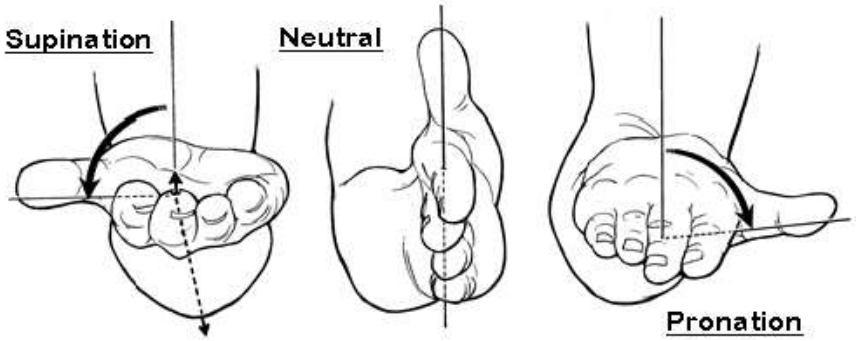

(c)

Figure 8: Various views of forearm rotation [34]. (a) Supination turns the palm up. (b) Pronation turns the palm down.

contact stresses, wear and tear during motion. Ligaments are short bands of tough tissue that hold the bones together and provide stability by restricting abnormal joint motion [38]. Ligaments at the elbow consist of the lateral collateral ligament (LCL) complex and the medial collateral ligament (MCL) complex (Fig. 4). Both of them hold the ulna, radius and humerus together and contribute to the elbow's stability by prevent excessive motion [31].

Ligaments at the wrist cover both the palm and the back of the hand (Fig. 5). Some of these ligaments connect the ulna and radius to the carpal bones, while others only link the carpal bones. Together the ligaments help stabilize the wrist joint, because the interlocking of bones is not sufficient to ensure joint stability [32]. Wrist ligaments are not very stretchable, constraining the movement of the wrist.

The interosseous membrane (IOM) is a major collection of soft tissues that span the forearm (Fig. 6). It is a complex and crucial structure responsible for forearm load sharing and stability [39]. The IOM can be divided into three portions, namely the distal portion

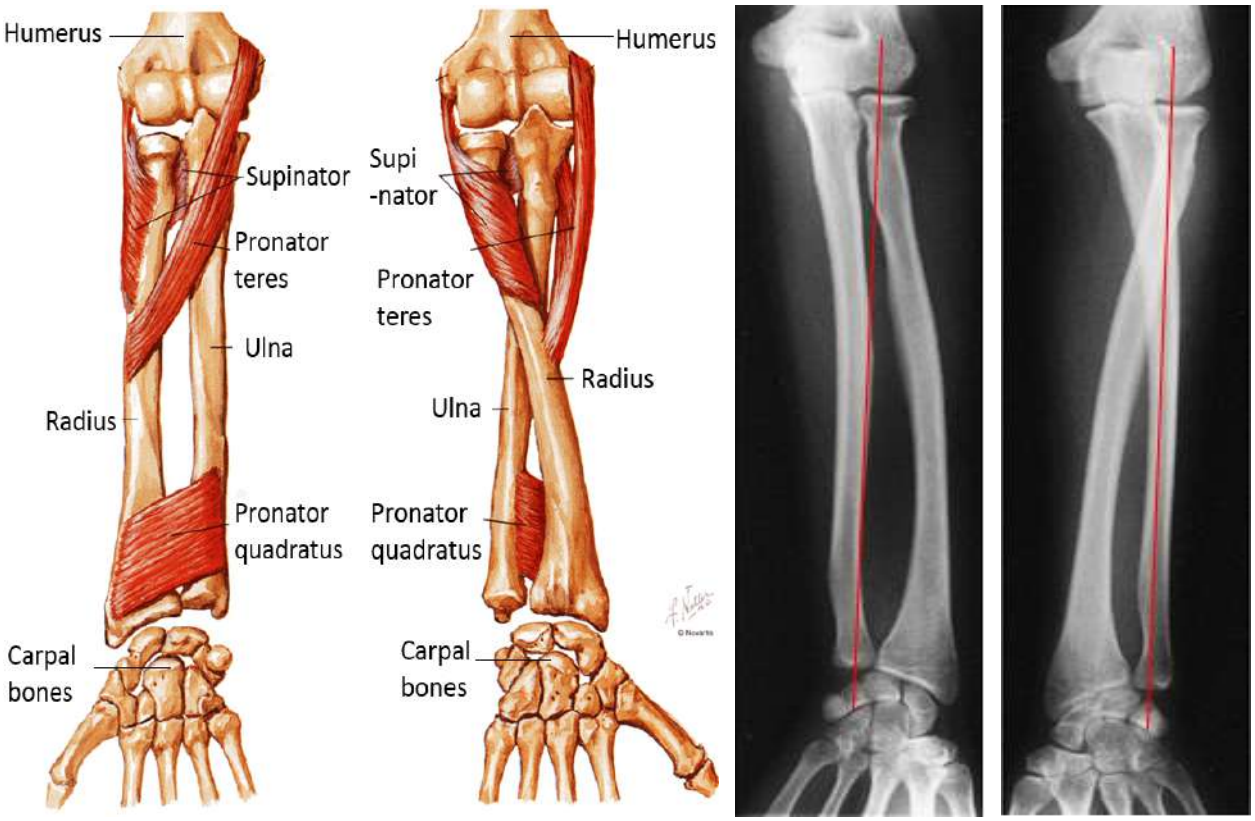

(a) (b) (c) (d)

Figure 9: Two directions of forearm rotation [35, 36]. (a, c) Supination rotates the forearm so the the palm faces up. (b, d) Pronation rotates the forearm so that the palm faces down. The red line indicates the rotation axis. This figure shows the various poses of the right forearm.

(near the wrist), the middle portion and the proximal portion (near the elbow). The distal and proximal portions are made up of soft and flexible tissue, while the middle portion consists of sturdy tissue [40]. The IOM's distal portion contributes to DRUJ stability in the forearm [41]. There is anatomical variation within the IOM (Fig. 7). The thickness of the distal portion varies widely among subjects [33]. Moreover, not every forearm has the distal oblique bundle (DOB) in the IOM.

2.2 Forearm Rotation

Forearm rotation is achieved by the rotation of the radius and the ulna relative to the humerus at the humeroulnar and humeroradial joints. It consists of two cases (Fig. 8). Pronation refers to the rotation of the forearm from palm up to neutral position to palm down. Supination refers to the rotation of the forearm from palm down to neutral position to palm up.

Forearm rotation is caused by the contraction of forearm muscles, namely pronator teres,

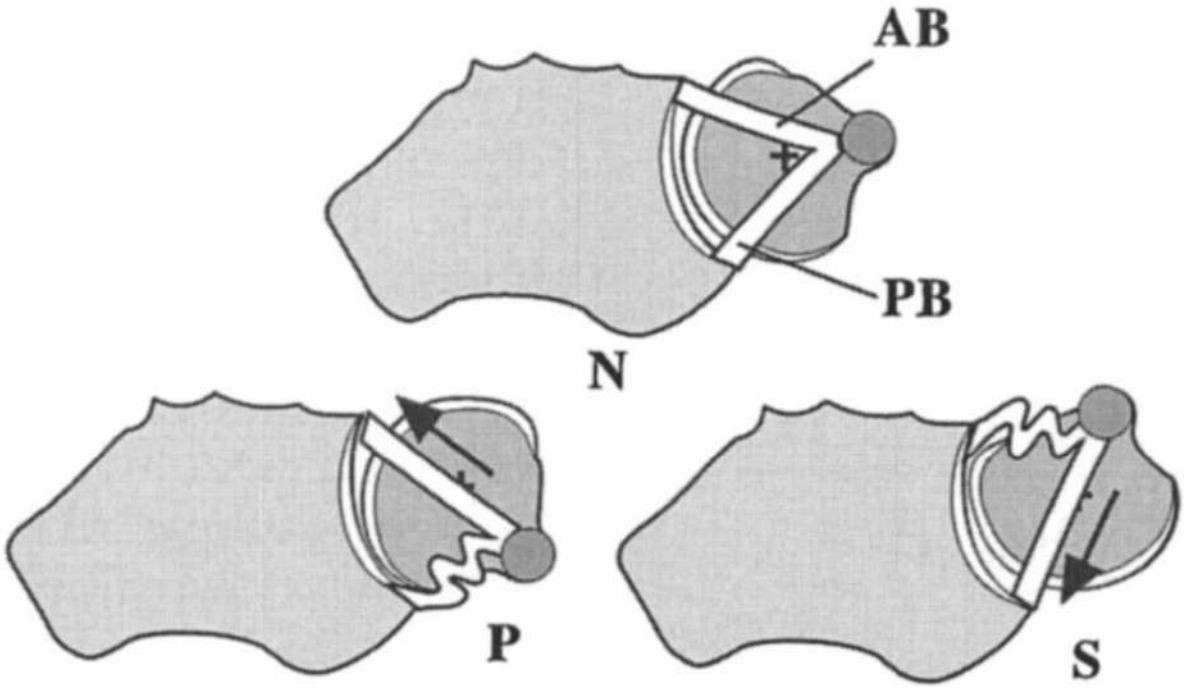

Figure 10: Motion of the radius relative to the ulna [42]. The radius rotates over the surface of the ulna. At the wrist joint, the ligaments PB and AB are equally stretched in neutral position (N). PB is tightened during pronation (P), while AB is tightened during supination (S). This figure shows the various poses of the left forearm.

pronator quadratus and supinator. Pronator teres has two heads, one attached to the humerus and the other to the ulna (Fig. 9). Its contraction pulls the middle part of the radius diagonally towards the opposite side of the humerus. Assisted by the contraction of pronator quadratus and constrained by the elbow joint, it causes the radius to rotate axially and cross over the ulna. Supinator arises from the supinator crest of the ulna and the lateral epicondyle of the humerus (Fig. 9). It wraps around the upper part of the radius and attaches to the radius along an oblique line. Its contraction, constrained by the elbow joint, causes the radius to rotate axially.

During forearm rotation, the radius rotates about a rotation axis that passes through two landmark points, namely the radial head center and the fovea of the ulnar head (Fig. 9c and 9d). The fovea of the ulnar head also happens to be its center. As the rotation axis is not parallel to the medial axis of the radius, the radius exhibits 3D rotation, including axial rotation. Unlike the radius, the ulna only rotates slightly in the mediolateral (sideway) direction and superior-inferior (up-down) direction about a single landmark point at the humeroulnar joint [42]. It does not rotate axially because of the trochlear notch that extends to the back of the humerus (Fig. 2b, 2c). Therefore, viewed along the direction of the forearm, the distal radius rotates axially over the surface of the ulnar head (Fig. 10). The gap between the distal radius and ulna surfaces is determined by the thickness of the cartilage between them.

In the past, the forearm was believed to rotate about a fixed axis relative to the radius

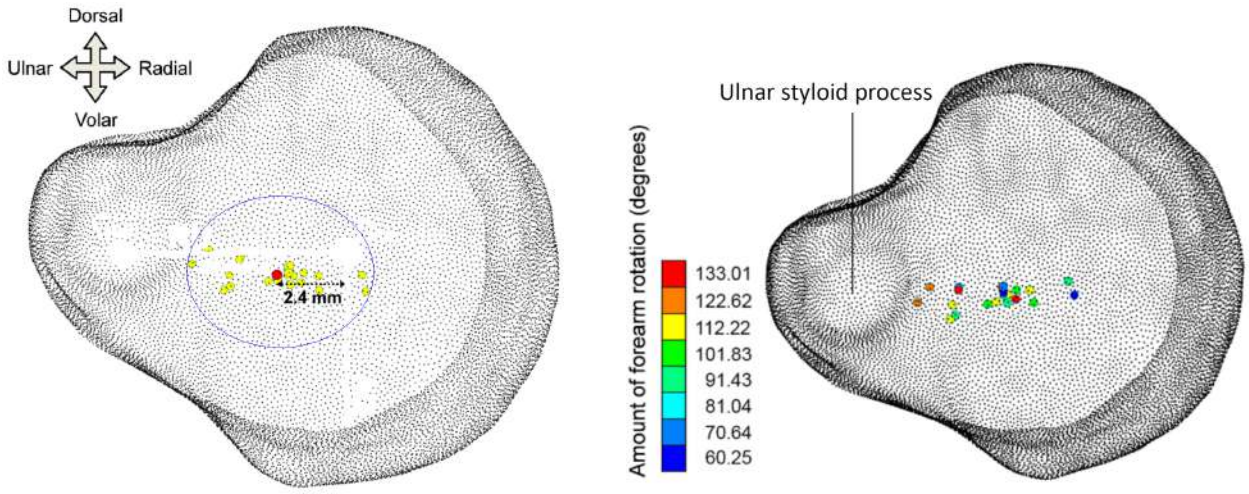

(a) (b)

Figure 11: Shifting of rotation centers on the ulnar head [16]. (a) Rotation centers (yellow dots) of 21 subjects with a circle showing uncertainty. (b) Shifting of rotation center during forearm rotation.

and ulna [44]. Later works reveal that the axis actually changes slightly during forearm rotation [8, 10, 13, 45, 46]. The points of intersection between the rotation axis and the surfaces of the radius and ulnar are called the rotation centers. The rotation center at the radial head remains virtually constant throughout forearm motion. In contrast, the rotation center at the ulnar head shifts towards the centroid of the ulnar styloid process during forearm rotation (Fig. 11) [16, 45]. Moreover, it varies across different subjects. There is some debate on when the rotation axis is furthest from the centroid of the ulnar head. [45] shows that the rotation axis is furthest from the centroid of the ulnar head when the forearm rotates from 30° of supination to 30° of pronation. However, [16] reports that the rotation axis is furthest from the centroid of the ulnar head when the forearm is at full pronation (Fig. 11).

As discussed, the ulna moves in a semi-lunar path [17, 47]. The position of the ulna during neutral position is considered to be 0°. During pronation, the ulna shows an average valgus shift (distal end pointing away from the torso midline) of 5.84°. During supination, the ulna shows an average varus shift (distal end pointing towards the torso midline) of 8.30°. In [47], it is reported that the ulna rotates about itself by approximately 3.2° during pronation and 0.5° during supination. However, in [48], it is reported that the ulna does not rotate about itself during forearm rotation.

Forearm rotation angle is usually defined as rotation of the radius with respect to the neutral (handshake) position of 0° (Fig. 8c), which is attained with the thumb pointing up and the palm facing sideways [49]. The neutral forearm position is also known as 0° of pronation and supination. The normal range of forearm rotation consists of 75° of pronation and 85° of supination [31]. The total range of rotation can be up to 180° [50].

The wrist joint rotates with the hand and forearm during forearm rotation. With the palm pressed firmly on a flat surface at supination or pronation, the forearm can rotate only

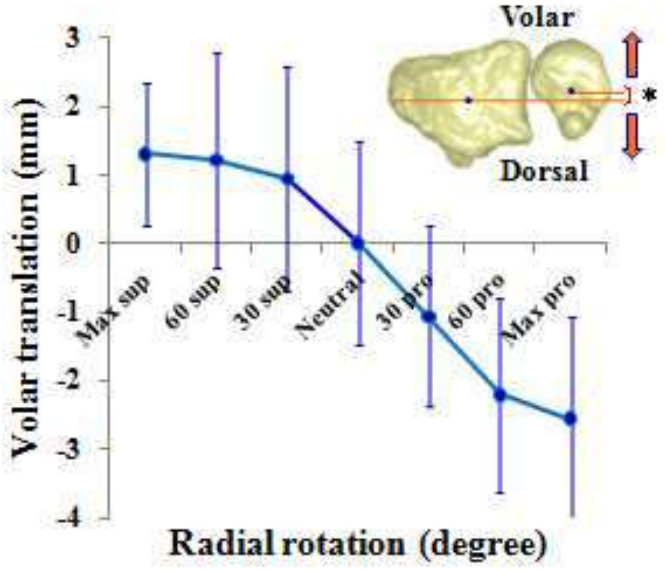

Figure 12: Ulnar head translation. The centroid of the ulnar head translates relative to centroid of the distal radius.

very slightly. In other words, during pronation and supination, the palm rotates with the forearm. There is no significant relative rotation between the forearm and the palm.

With the forearm bent, the forearm can pronate and supinate beyond the normal range. This is not caused by the forearm muscles, but rather the rotation of the humerus [51]. At the extreme of normal forearm rotation, the elbow joint is locked. Once this happens, the forearm simply follows the rotation of the humerus.

During forearm rotation, the ulnar head centroid moves relative to the distal radius (Fig. 12) [45]. The ulnar head centroid is located at approximately 2.6 mm dorsal (towards the palm) at maximum pronation. The ulnar head centroid moves a total of around 4 mm during forearm rotation. The ulnar head usually moves dorsal in pronation and volar (towards the back of the palm) in supination [8, 45].

The radius also moves proximally or distally when the forearm rotates. In general, the radius translates towards the elbow joint during pronation and shifts towards the wrist joint during supination [10, 31]. However, for some subjects, it is possible that the radius migrates almost exclusively towards the elbow during forearm rotation [52]. For the general case, the radius' average translation in either direction is reported to be 1.3 mm [53]. The relationship between forearm rotation angle and radius translation remains uncertain. According to [54], there is a large change in the position of the radius between mid-supination and mid-pronation. This rotation arc accounts for 80% of total radius translation. However, in [53], radius translation seems to follow a linear relationship, with the radius translating along the ulna by 0.08 mm for every 10° of supination. Furthermore, radius translation during forearm rotation is influenced by the presence of the DOB structure in the forearm's IOM [55]. Radius translation occurs more during forearm rotation when the IOM does not have the DOB.

The radial head demonstrates slight motion during forearm rotation. According to [56],

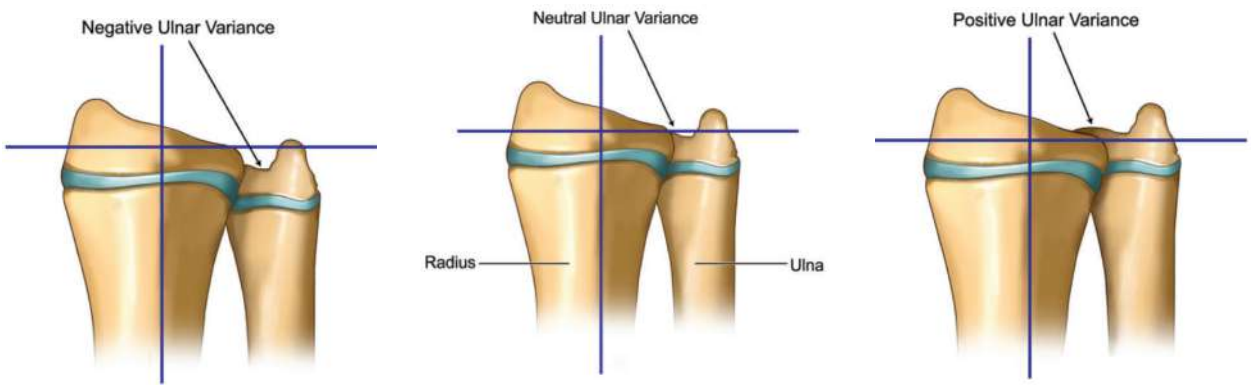

(a) (b) (c)

Figure 13: Ulnar variance [43]. (a) Ulna is closer to elbow joint. (b) Ulna and radius are on the same level. (c) Ulna is closer to wrist joint.

Table 1: Average length of IOM ligaments (in mm) [4].

Position	DOB	AB	CB	DOAC	POC
Pronation	25.9 ± 3.0	20.5 ± 2.8	30.8 ± 4.1	29.2 ± 4.7	30.6 ± 5.4
Neutral	26.0 ± 3.4	22.5 ± 3.0	31.4 ± 3.8	28.2 ± 4.6	26.5 ± 4.7
Supination	25.4 ± 3.1	22.6 ± 3.3	31.5 ± 4.1	24.5 ± 3.8	26.4 ± 4.2

the radial head center moves posteriorly in neutral and anteriorly in pronation. According to [57], the radial head center moves posteriorly and medially during supination. It moves anteriorly and laterally during pronation. Overall, the radial head center mostly demonstrates anteroposterior motion during forearm rotation.

Radius translation during forearm rotation can affect ulnar variance. Ulnar variance refers to the difference in height between the joint surfaces of the distal radius and ulna (Fig. 13) [58]. Neutral variance means both the ulnar and radial articulating surfaces are at the same level. Positive variance means the ulna projects more towards the wrist, and negative variance means the ulna projects more towards the elbow. Ulnar variance decreases as the forearm is rotated from pronation to supination [59]. Mean normal ulnar variance in neutral rotation is approximately 0.74 mm $\pm$ 1.46 mm [60]. Maximum ulnar variance measured during gripping in pronation is approximately 1.52 mm $\pm$ 1.56 mm. Minimum ulnar variance measured when forearm is relaxed in supination is approximately 0.19 mm $\pm$ 1.43 mm. In all cases for a healthy forearm, ulnar variance is small. Significantly positive or negative ulnar variance can lead to forearm problems affecting normal rotation.

The IOM changes length during forearm rotation. The extent of such length change remains a debate. According to [61, 62, 63, 64], the IOM's proximal and distal portions show dynamic changes during forearm rotation, while the IOM's middle portion demonstrates minimal changes. The IOM's middle portion is stretched to its maximum at 22° of supination. It remains taut during forearm rotation to provide stability between the radius and the ulna. The proximal and distal portions stretch more to facilitate smooth rotation.

According to [65], the distal, middle, and proximal portions of the IOM demonstrate similar length change. They stretch the most in neutral position and the least in full prona-

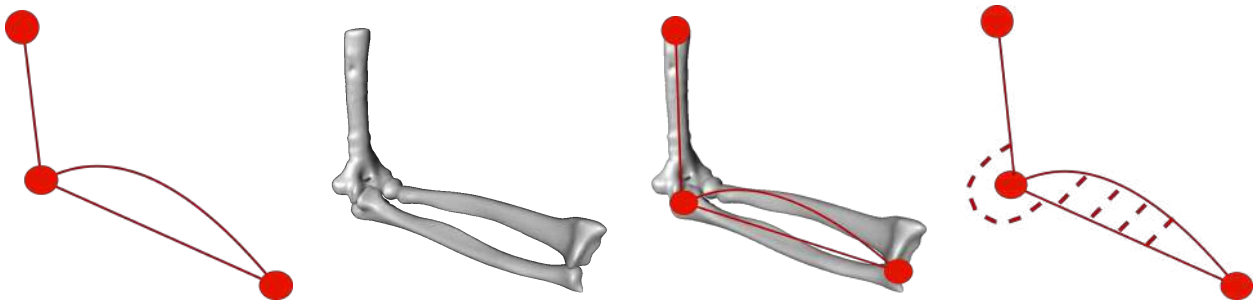

(a) (b) (c) (d)

Figure 14: Types of forearm model. (a) Abstract model. (b) Geometrical model. (c) Geometrical model aligned to abstract model. (d) Abstract model with soft tissues (dotted lines).

tion. Because they stretch the least in full pronation, they exhibit minimal tension in that position.

However, as shown in [4], the IOM's proximal portion shows more dynamic length changes during forearm rotation than do its distal and middle portions (Table 1). Specifically, the AB, CB and DOB ligaments show smaller length changes and serve as the forearm's stabilizers, while the DOAC and POC demonstrate more substantial length changes during forearm rotation. While the exact role of the DOAC and POC remains unconfirmed, these two structures are believed to help restrain excessive forearm pronation.

3 Existing Work

Modeling forearm motion involves creating a computational model to generate continuous forearm motion. Existing work on modeling forearm rotation can be grouped into several categories, namely, abstract models, static models, kinematic models and dynamic models. Abstract models describe joints as points and bones as straight lines connecting the points (Fig. 14a). They do not model 3D bone geometry, soft tissue and interactions between bones and soft tissue. So, they are omitted in the following discussion. Nevertheless, they are used as a fundamental component of kinematic and dynamic models. This section focuses on static models, kinematic models and dynamic models, which model 3D bone geometry.

3.1 Static Models

Static models [4, 5, 6, 7, 8, 9, 10, 11, 12, 13, 14, 15, 16, 17, 18, 19] consist of a sequence of geometrical models (Fig. 14b) of 3D bones at discrete poses. Methods applying static models first use imaging techniques such as computer tomography (CT) or 4D computer tomography (4DCT) to scan the forearm at a sequence of discrete poses. Then, they segment the bone regions in the scans and construct 3D bone models from the segmented regions.

Static models can also model soft tissue. For example, the methods in [4, 14, 15, 66] model IOM thickness, stiffness, length change and other properties during forearm rotation by simulating IOM structures as straight lines connecting defined attachment locations. The

method in [9] models wrist ligaments during forearm rotation also as straight lines connecting attachment locations. These works compute the 3D shortest paths between attachment locations to model soft tissue length.

Static models have three main advantages. They are subject-specific because they are constructed from a subject's CT scans. They can also model soft tissues. They are straightforward to construct, since only two steps, namely segmentation and 3D surface recovery, are needed to create a static model once a patient's CT scans are available.

Static models have several drawbacks. They cannot model continuous bone motion. They also require multiple CT scans at multiple discrete poses. The former can increase the risk of radiation-induced cancer [67], whereas the latter is costly. Therefore, static models are not feasible for routine clinical applications.

3.2 Kinematic Models

Kinematic models [7, 11, 20, 21, 22, 23, 24] consist of a single abstract model at neutral pose and joint motion data over the motion range, without considering forces. In addition, they can include a geometrical model of the bones aligned to the abstract model (Fig. 14c). In general, they describe the motion of a kinematic chain of more than one link connected at multiple joints and end-effectors. Kinematic models consist of two stages, namely **parameter estimation** and **motion generation**. In the parameter estimation stage, forearm motion data over a range of bone poses are captured using various techniques such as fluoroscopy [45, 68, 69, 70, 71], 4D computer tomography (4DCT) [18, 19], 4D rotational x-ray (4DRX) [24, 72] and motion capture (mocap) [20, 21, 73, 74]. Then, depending on the technique used to capture motion data, appropriate procedures are applied to estimate model parameter values from the acquired forearm motion data. The parameter values include properties such as bone length, coordinate axes and joint angles as a function of time. In the motion generation stage, forward kinematics is applied on the abstract model with joint angles to compute abstract bone poses, i.e., the positions of joints and end-effectors, as a function of time (Fig. 15). Then, a 3D bone model is fitted to the computed abstract bone poses to obtain 3D bone poses over a range of motion.

Kinematic models vary in the way their parameters are estimated. Existing methods for estimating the parameters of kinematic models can be categorized as either direct measurement and inverse kinematics. Direct measurement involves measuring bone lengths at neutral pose and joint angles at other poses relative to neutral pose. It can be accomplished by 3D-model-to-3D-model registration, 3D-model-to-3D-image registration or 3D-model-to-2D-image registration, depending on the motion data type.

The methods in [4, 6, 7, 8, 9, 10, 11, 12, 13, 14, 17, 18, 19, 75] perform 3D-model-to-3D-model registration. First, they capture the forearm at various poses using either multiple static CT scans or a time series of CT scans (4DCT). Then, they segment the scans to obtain a 3D model of the forearm at each pose, which corresponds to a series of static models. Next, they apply 3D-model-to-3D-model registration to register the 3D model at neutral pose, called the reference model, to the 3D model at each other pose. This involves changing the poses of the bones in the reference model to align to those in the other poses. The amount of change gives the rotation and translation of the bones, which constitute the motion parameters. Among these existing works, [7, 11] develop complete kinematic models;

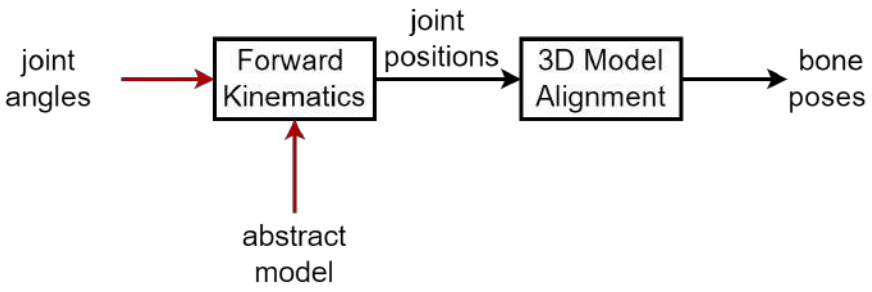

Figure 15: The motion generation stage of kinematic models. It takes joint angles as inputs and generate bone poses.

the others only measure model parameters.

The methods in [24, 70] perform 3D-model-to-3D-image registration. First, they capture a static CT or 3D rotational x-ray (3DRX) of the forearm at neutral pose and a 4D rotational x-ray (4DRX) scan of the forearm during motion. A 3DRX scan involves a C-arm that rotates in a semicircular arc around the forearm, taking multiple x-ray images of the forearm at one particular pose. The x-ray images captured for each forearm pose are then converted to a single 3D image, which is equivalent to a static CT scan, using an algorithm similar to CT imaging [76]. A 4DRX scan is a time series of 3DRX scans, which involves repeating the 3DRX scan every time the forearm moves to another pose [72]. Once both the static scan and 4DRX scan are available, the methods in [24, 70] first construct a 3D model of the forearm by segmenting the static CT or 3DRX scan at neutral pose. They then perform 3D-model-to-3D-image registration by aligning the 3D model with each 3D image of the 4DRX sequence. Like 3D-model-to-3D-model registration, this involves changing the poses of the bones in the 3D model to align with those in the 3D images, thus recovering motion parameters. Among these existing works, [24] develops a complete kinematic model; the other works only measure model parameters.

The methods in [45, 68, 69, 71] perform 3D-model-to-2D-image registration. First, they capture a static CT scan of the forearm at neutral pose and a fluoroscopic (x-ray) video of the forearm over a range of bone poses. A fluoroscopic video is a sequence of 2D x-ray images. Next, they segment the static CT scan to obtain a 3D model of the forearm at neutral pose. After that, they iteratively change the poses of the bones in the 3D model and obtain each pose's digitally reconstructed radiographs (DRRs), which are simulations of x-ray obtained by performing 3D-to-2D projection through the CT volume [77]. They apply 2D-image-to-2D-image registration by matching each DRR to a fluoroscopic video frame. The amount of pose change that produces the best matching DRR gives the rotation and translation of the bones, which constitute the motion parameters.

Instead of direct measurement, some methods [20, 21, 22, 23, 74] apply inverse kinematics for parameter estimation. These methods use a motion capture (mocap) system involving markers attached to a subject's forearm. First, they capture a neutral pose of the forearm by recording the positions of the markers. Next, they use the marker positions at neutral pose to estimate the model parameters, which include abstract bone length and joint angles at neutral pose. Then, they capture the marker positions during forearm motion to obtain

mocap data. Finally, they apply inverse kinematics on the mocap data to obtain motion parameters over a sequence of poses. Among these existing works, [20, 21, 22, 23] develop complete kinematic models; the rest only measure model parameters.

Kinematic models can also model soft tissues as lines or curves connecting attachment sites (Fig. 14d). As the model changes pose, the lengths of the soft tissues can be measured using the methods in [4, 6, 14, 74].

Kinematic models are subject-specific because they contain a subject's 3D bone model extracted from CT or 3DRX. They can model forearm bone poses over a range of motion. Moreover, they can model soft tissue during continuous motion.

Kinematic models are more complex than static models due to the application of additional procedures such as 3D-model-to-3D-model registration, 3D-model-to-image registration and inverse kinematics. Methods involving mocap systems are susceptible to marker position errors because the markers and the bone do not move rigidly with respect to each other as the skin deforms [78]. Methods involving mocap systems are not feasible for routine surgery planning as reflective markers need to be attached to the subject, which is a tedious and time-consuming process. Methods using multiple static CT scans, 4DCT, 4DRX and fluoroscopy expose the subject to excessive radiation. Therefore, kinematic models are more suitable for medical research performed on cadaveric bones and not feasible for routine surgery planning.

3.3 Dynamic Models

Dynamic models describe 3D bone poses and forces over a range of motion. Only one method that uses a dynamic model for forearm rotation has been found [79]. The others employ dynamic models to describe motion and forces for elbow flexion and extension [25, 26, 27, 28, 29, 30]. In principle, they can be modified to model forearm rotation.

A basic dynamic model [79] consists of a muscle model, a musculoskeletal model and a forward dynamic model (Fig. 16). The muscle model describes the muscles attached to the bones. There are many muscle models in the literature. Among them, the Hill-type model is the most widely used in biomechanical studies [80]. It relates muscle activation values to muscle forces. Its parameters, such as muscle length, are measured in biomechanical studies involving real muscle tissues [81].

The musculoskeletal model includes an abstract bone model. It computes joint moments given muscle forces obtained from the Hill-type muscle model. Joint moment (also referred to as joint torque) is a measure of the tendency of an exerted force to cause a joint to rotate about a specific axis [82]. Joint moment is defined as the product of the muscle force and the moment arm, which is the perpendicular distance between the line of action of the muscle force and the axis of rotation. The line of action of a force is a straight line along which the force acts.

Given the joint moments, the forward dynamic model applies forward dynamics to drive the abstract model from one state to the next. At every state, the positions of the joints and end-effectors are computed. Finally, a 3D bone model is aligned to the abstract bone poses to produce 3D bone poses.

The computed joint moments can be compared with measured joint moments to refine a basic model's parameters. To this end, the method in [83] applies inverse dynamics on

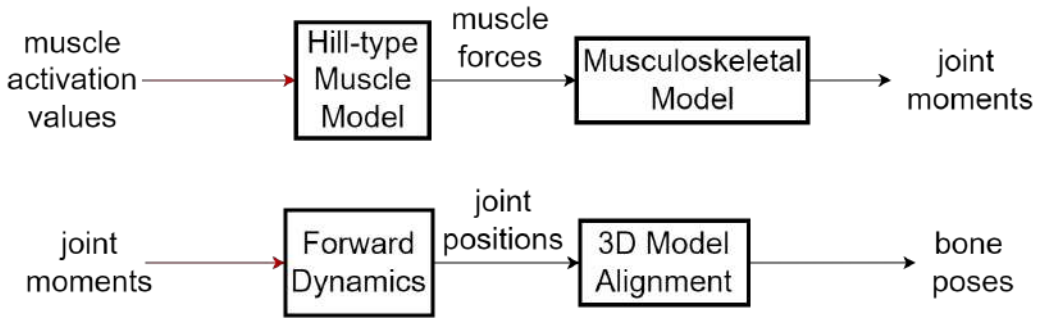

Figure 16: Basic dynamic model. It computes joint moments from muscle activation values and uses the joint moments to compute bone poses.

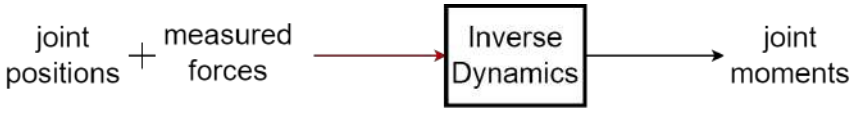

Figure 17: Parameter estimation for dynamic model. Inverse dynamics is used to compute joint moments from joint positions and measured forces.

mocap data and measured forces to obtain measured joint moments (Fig. 17). After that, it compares the measured joint moments obtained from inverse dynamics with the joint moments computed from the musculoskeletal model. It uses the error between the measured and computed joint moments to refine the model parameters.

Similar to kinematic models, dynamic models also consist of two stages, namely **parameter estimation** and **motion generation**. During the parameter estimation stage, the parameters of the Hill-type muscle model and musculoskeletal model are estimated empirically. During the motion generation stage, muscle activation values are used to generate bone poses through a sequence of models, as described in the previous paragraphs.

Existing dynamic models differ mainly in the way they generate joint moments. The basic dynamic model requires the user to provide muscle activation values (Fig. 16), which are difficult to estimate. To overcome this difficulty, the methods in [25, 26, 27, 28] use **electromyography (EMG)** to record the electrical activity of muscle tissue, using electrodes attached to the skin or inserted into the muscle [84]. Next, they employ a muscle activation model to convert EMG signals to muscle activation values that feed into a basic dynamic model (Fig. 18).

Some EMG-driven methods [29, 85, 86, 87] employ **neural networks** to replace the muscle activation model, Hill-type muscle model and the musculoskeletal model. They train the neural networks to produce joint moments given EMG signals. Among these existing works, [29] develops a complete dynamic model; the rest only estimate joint moments given EMG signals.

EMG signals must be captured experimentally, which is inconvenient for practical applications. To resolve this difficulty, the Computed Muscle Control (CMC) model introduces a dynamic controller to generate control signals that replace EMG signals (Fig. 19) [88]. The method in [30] uses the CMC model to model elbow flexion and extension.

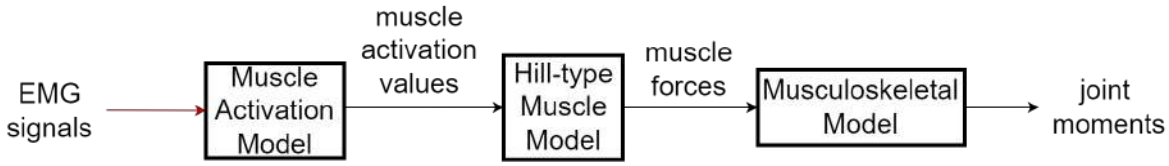

Figure 18: EMG-driven dynamic model. It uses a muscle activation model to convert EMG signals to muscle activation values that feed into a basic dynamic model.

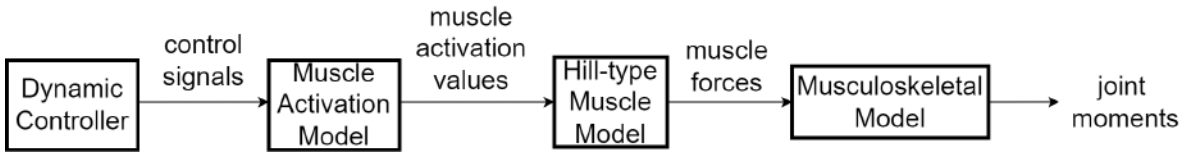

Figure 19: CMC dynamic model. It uses a dynamic controller to generate control signals that replace EMG signals in the EMG-driven model.

Dynamic models are not suitable for surgical planning. They require the moment arms and lines of action that are challenging to measure in both cadavers and living patients [83]. They are able to compute muscle forces, and hence joint moments, but it is usually not possible to verify whether the computations are correct. Moreover, they often involve high computational costs and may also require cumbersome mocap and EMG systems, which are not feasible for routine clinical practice.

Dynamic models can also model the interactions of soft tissues other than muscles and tendons. The methods in [89, 90, 91] provide finite element models that incorporate soft tissues such as cartilages, ligaments and IOM structures. These methods can compute results such as muscle, ligament, and articular surface contact forces. They also model contact pressure between forearm cartilages.

Dynamic models can be subject-specific, provided that both 3D bone geometry and muscle model of the subject are available. Dynamic models can describe bone poses during continuous motion as well as forces exerted by soft tissues such as muscles and tendons.

Dynamic models are more sophisticated than static and kinematic models. Unlike static and kinematic models, they also describe forces. Methods adopting dynamic models often use complex procedures such as inverse or forward dynamics along with EMG and mocap systems. They may also use neural networks, which require data collection and training. Given the extra complexity, they are not feasible for routine clinical application of surgery planning.

3.4 Summary

Table 2 compares existing works for modeling forearm rotation. Major variants of kinematic models differ in the way they estimate model parameters, but they apply the same motion generation method. On the other hand, major variants of dynamic models differ in the way they compute muscle activation values and joint moments. Consequently, their parameter estimation methods can differ accordingly.

Table 2: Comparison of existing models of forearm rotation.

Model	**Major variants**	**# static CT**	**Param estimation**	**Soft tissue**	**Subject-specific**	**Model complexity**	**Clinical usage**
Static	nil	> 1	nil	Possible	Yes	Low	No
Kinematic	Inverse kinematics	1	Motion capture data	Possible	Yes	High	No
	3D-model-3D-model	≥ 1	4DCT	Possible	Yes	High	No
	3D-model-3D-image	1	4DRX, 3DRX	Possible	Yes	High	No
	2D-image-2D-image	1	X-ray video	Possible	Yes	High	No
Dynamic	Basic	1	various	Yes	Possible	High	No
	EMG-driven	1	EMG + various	Yes	Possible	High	No
	CMC	1	Various	Yes	Possible	High	No
	Neural network	1	EMG + Various	Yes	Possible	High	No
Proposed	nil	1	Minimum	Possible	Yes	Low	Yes

A static model uses multiple CT scans to construct the 3D bone models at various poses, making it subject-specific. It can model soft tissues. It has low complexity because it does not require parameter estimation. However, it is not suitable for clinical usage due to excessive radiation exposure from multiple CT scans.

A kinematic model uses various imaging and registration techniques to obtain 3D bone models over a range of motion. It is subject-specific because it uses a CT scan to obtain a 3D model bone model at neutral pose. It can also model soft tissues. It is complex because it requires parameter estimation, which varies depending on the variant. It is not suitable for clinical usage due to high complexity and excessive radiation exposure from various imaging techniques.

A dynamic model describes 3D bone poses and forces over a range of motion by using a muscle model, a musculoskeletal model and a forward dynamic model. It can be subject-specific, if a subject's bone and muscle geometries are available. It models the interaction of soft tissues to describe forces. It is sophisticated because it involves parameter estimation and complex procedures such as inverse or forward dynamics. It is not suitable for clinical usage due to its high complexity and potential need for EMG and mocap systems.

The proposed method uses a single CT scan to construct a functional model for forearm rotation. The model is subject-specific and has the potential of modeling the effects of soft tissues. As a first approximation, this QE paper omits soft tissues. Requiring minimal parameter estimation, the proposed model is expected to be straightforward to develop and

feasible for routine clinical usage.

4 Preliminary Work

The overall goal of this research is to develop a subject-specific forearm rotation model for routine clinical applications. This involves two components: (1) building a subject-specific forearm bone model and (2) estimation of forearm bone poses over a range of forearm rotation.

4.1 Problem Formulation

Building a subject-specific forearm bone model involves segmenting a CT scan and constructing 3D forearm bone geometries at a particular pose. These steps are relatively simple and are omitted in this section. Estimation of forearm bone poses during forearm rotation is the most significant component. It can be defined as follows:

> Given a geometrical model of the forearm at neutral pose, generate the poses of the radius and ulna with respect to the humerus over the range of rotation subject to wrist joint constraint, elbow joint constraint and IOM constraint.

The geometric model of the forearm consists of the radius, ulnar, hand bones and part of the humerus. As discussed in Section 2, the forearm has a normal rotation range of about 160° on average, which consists of approximately 75° of pronation and 85° of supination. In the absence of humeral rotation, the forearm cannot rotate beyond the normal range.

The wrist joint constraint requires that, as the forearm rotates, the hand bones rotate along with the radius. Moreover, the distal radius rotates across the surface of the ulnar head, to satisfy the DRUJ constraint. The DRUJ constraint requires the distal radius and ulnar head to maintain an approximately constant gap determined by the thickness of the cartilage between them. The flexing of hand bones up and down with respect to the wrist is omitted in forearm rotation.

The elbow joint constraint requires that the radius rotate about a rotation center located at the humeroradial joint (HRJ) (Fig. 20a) and the ulna rotates about a rotation center located at the humeroulnar joint (HUJ) (Fig. 20b and 20c). Specifically, the radius' rotation center is at the radial head center, while the ulna's rotation center is located in the space above the trochlear notch. The gaps between the humerus and the radius and ulna are approximately constant.

The IOM can also constrain the movement of the forearm. Different parts of the IOM can stretch by different amounts [4]. The DOB, AB and CB demonstrate the least amount of length change, limiting forearm motion. The DOAC and the POC are more flexible with larger length changes.

The general problem of modeling forearm rotation is a challenging problem due to all the constraints. It can be simplified into various versions, in increasing order of complexity:

1. Geometrical model with stationary ulna

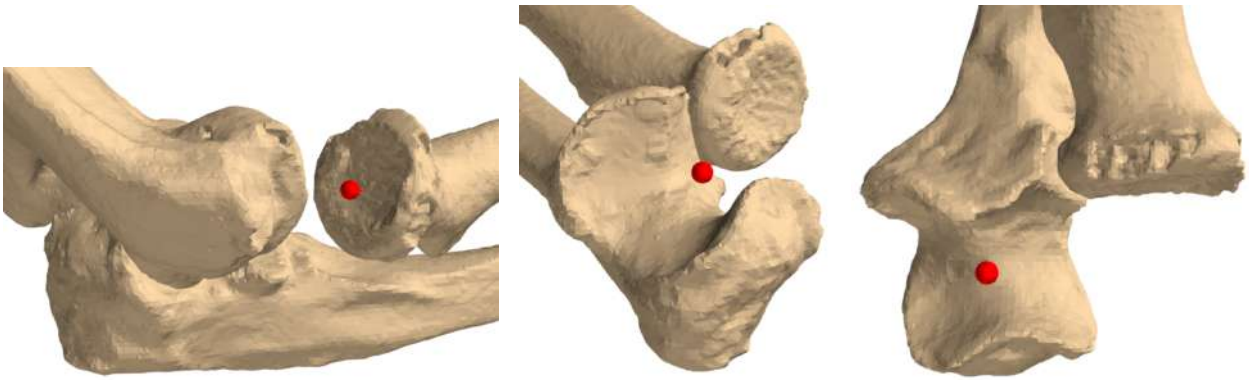

(a) (b) (c)

Figure 20: Landmark points for radius and ulna motion. (a) Landmark point at the radial head center functions as the rotation center of radius rotation. In this figure, the radius is pulled forward to facilitate viewing of its landmark point. (b, c) Landmark point above the ulna's trochlear notch functions as the rotation center of ulna rotation.

This is the simplest version of the problem and is modeled entirely based on geometrical considerations. In this version, the ulna is stationary and the radius rotates about a fixed rotation axis, along with the hand bones. This version is not expected to produce accurate forearm rotation. Nevertheless, many existing works adopt this model due to its simplicity [4, 5, 6, 8, 9, 10, 11, 13, 14, 15, 16, 19].

2. Quasi-physiological model with stationary ulna

   This version models radius rotation by emulating the effects of the pronator and supinator muscles. For simplicity, the ulna remains stationary in this model. Although there are previous works that measure the effects of forearm rotation on soft tissue length change [4, 6, 14, 15], thus far, no previous work that solves this version of the problem has been found.

3. Geometrical model with moving ulna

   This version generalizes Version 1 to include the semi-lunar motion of the ulna. In this case, the rotation axis of the radius shifts along with ulna motion so that the radius surface remains in contact with the ulnar surface. The method in [7] solves this version of the problem with two static CT scans.

4. Physiological model with moving ulna

   This version generalizes Version 2 to include the semi-lunar motion of the ulna by modeling muscles, cartilage, ligaments and IOM structures and their real-time interactions as actual causes of forearm rotation. Thus far, no previous work that solves this version of the problem has been found.

This QE paper presents solutions for solving versions 1 to 2. Version 3 and 4 are more elaborate and are left out of this QE paper. Each solution takes the 3D models of the hand

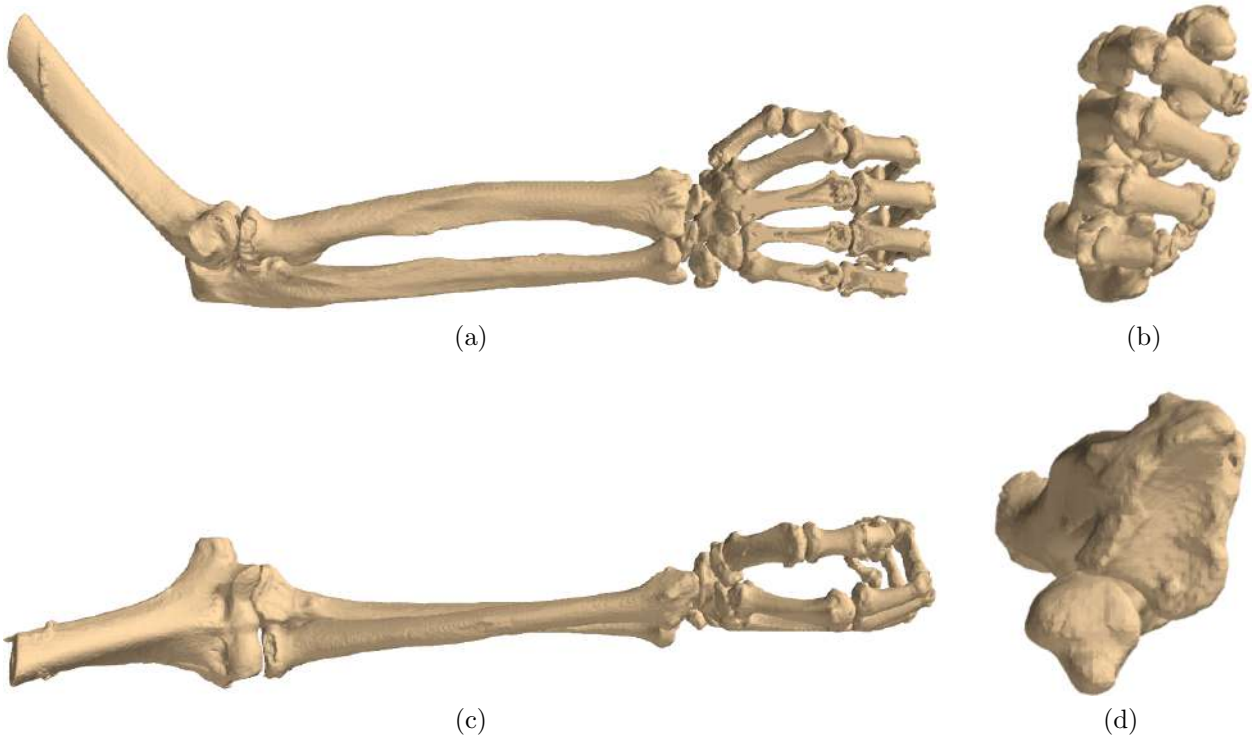

Figure 21: Forearm bone models at initial pose. (a) Side view. (b) Frontal view with hand bones. (c) Top-down view. (d) Frontal view with hand bones and humerus omitted to visualize distal radius and ulna.

bones, radius, ulna and part of the humerus at a particular pose as inputs (Fig. 21). Due to the limited resolution of the CT scan, not all bone surfaces are recovered, in particular, the small surfaces at the finger joints. Therefore, it is not possible to use bone surface to model forearm rotation. Solutions in this QE paper are implemented using Python and the scientific 3D visualization library PyVista [92].

4.2 Geometrical Model with Stationary Ulna

4.2.1 Computational Method

The initial pose of the bone models obtained from a CT scan is not necessarily the neutral pose (Fig. 21d). To indicate the range of forearm rotation, a pair of landmark points are placed at distinctive points on the distal radius surface and distal ulna surface (Fig. 22). The alignment of the blue points indicate the approximate full supination pose. The alignment of the red points indicate the approximate full pronation pose.

The radius and hand bones are rotated as a single rigid object about a fixed rotation axis. The rotation axis is defined by a straight line passing through the center of the radial head and the ulnar head center. The radius and hand bones are rotated in increments of θ degrees from the initial pose to full pronation (Fig. 22). Next, it is rotated from full pronation to full supination (Fig. 22) and then back to an approximate neutral pose. Throughout the

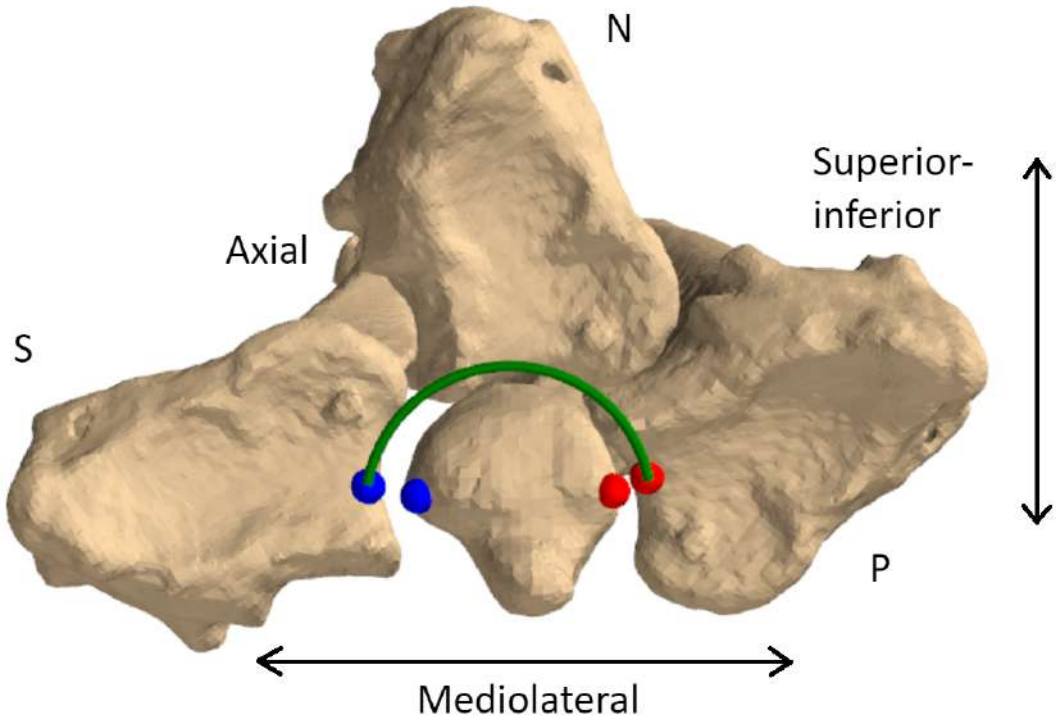

Figure 22: Relative poses of radius and ulna during forearm rotation with the ulna fixed. P: full pronation pose. N: approximate neutral pose. S: full supination pose. This figure shows the various poses of the right forearm.

rotation, the ulna and humerus remain stationary. The rotation of the radius and hand bones is performed using PyVista's `rotate_vector` function, which implements Rodrigues' rotation formula that rotates 3D points about a vector.

4.2.2 Results and Discussions

The radius and hand bones rotate about the rotation axis, while the ulna and humerus are stationary in this version (Fig. 23). The bones rotate with no collision. At the wrist joint, the radius rotates about the ulnar head center. At the elbow joint, the radius rotates about the radial head center. These two rotation centers are stationary throughout forearm rotation in this version.

The wrist joint constraint is only partially satisfied in this version. Although there is no bone collision at the wrist joint, the gap of the distal radioulnar joint is not maintained, especially during supination. This occurs because the ulna does not move along with the radius and hand bones. The gap is smaller and more stable during pronation.

Similarly, the elbow joint constraint is only partially satisfied. In particular, the constraints on the humeroradial joint and humeroulnar joint are satisfied because the rotation center of the radius is fixed and the ulna is stationary. But the gap of the proximal radioulnar joint is not maintained.

The methods in [5, 19] adopt this version, while the methods in [4, 6, 8, 9, 10, 11, 13, 14,

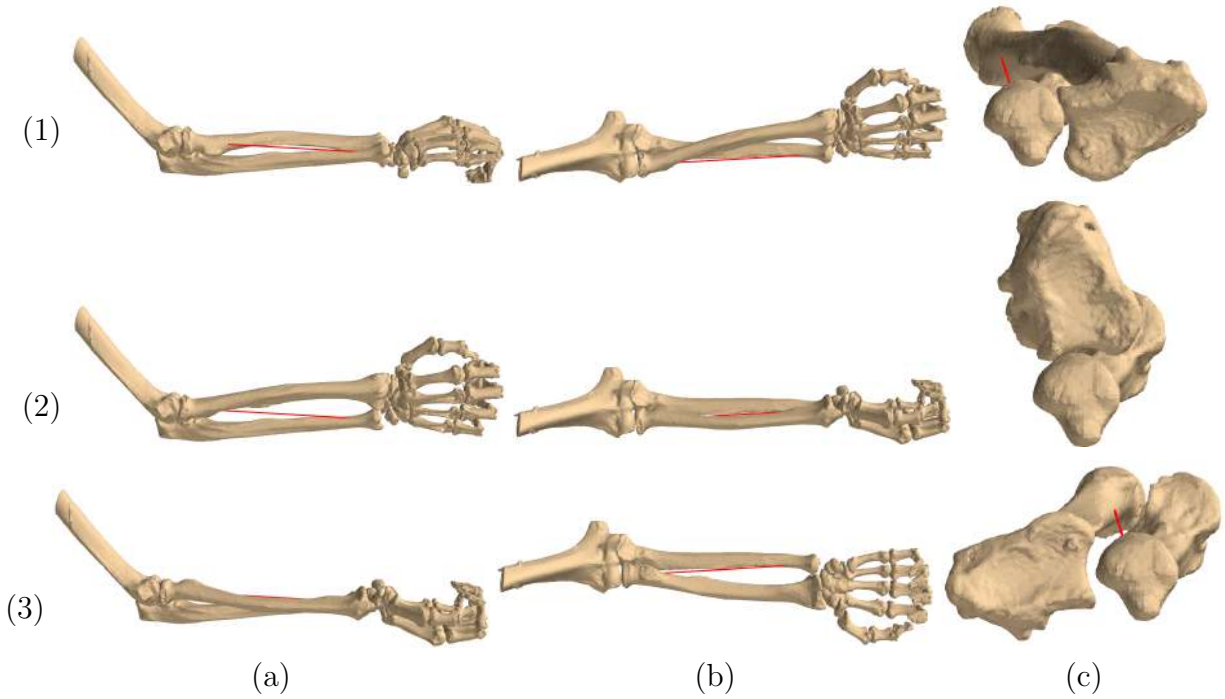

Figure 23: Results of Version 1. (1) Full pronation. (2) Approximate neutral pose. (3) Full supination. (a) Side view. (b) Top-down view. (c) Frontal view without humerus and hand bones.

15, 16] adopt a modified version of this version by omitting both the humerus and the hand bones. Although this version may be sufficient for the purposes of these previous works, it is not accurate and feasible to be used for routine surgical planning. It is reproduced in this paper for the purpose of comparison.

4.3 Quasi-physiological Model with Stationary Ulna

4.3.1 Computational Method

In this version, forearm rotation is generated by the approximation of muscle contraction to drive the motion of the radius and hand bones. It is a quasi-physiological model because it models the net effects of the muscles rather than the exact action of each muscle. Compared to Version 1, it has the advantage of not requiring the radius rotation axis to be fixed geometrically. In this version, the hand bones rotate with the radius, while the ulna and humerus are stationary.

The major muscles involved in forearm rotation include the pronator teres (PT, Fig. 24 red vectors) that pronates the radius, and the supinator (S, Fig. 24 green vectors) muscle that supinates the radius. Each muscle is modeled by a force vector tangential to the bone surface, effected by the muscle at each of its attachment points. As an approximation of radius motion, the tangential force vector is expected to pull each attachment point in the mediolateral or superior-inferior position. The tangential force vector does not act in the

(a) (b)

Figure 24: Instantaneous force vectors tangential to bone surface at attachment points for PT (red), DRUJ (blue) and S (green). The forearm is shown at initial position. The vectors are drawn not to scale.

forearm's axial direction, as the radius does not translate in that direction during forearm rotation. Pronation force vectors are zero during supination, and supination force vectors are zero during pronation. In addition, an additional force (Fig. 24, blue vectors) is used to emulate the constraint imposed by the distal radioulnar joint (DRUJ), which maintains a constant gap between distal radius and distal ulna.

In theory, the DRUJ can be emulated as a constraint on rigid rotation rather than as a force vector. However, this approach leads to a constrained rotation problem that is harder to solve. So, as a first approximation, DRUJ is included as a force vector, leading to an unconstrained rotation problem that is easier to solve.

Let $\mathbf{f}_i$ be the force vector associated with each attachment point. At each time step of forearm rotation, the force vector moves an attachment point $\boldsymbol{p}_i$ to its desired location $\mathbf{q}_i$ along the force direction by an amount equivalent to its magnitude:

$$\mathbf{q}_i = \mathbf{p}_i + \mathbf{f}_i. \tag{1}$$

As the radius is a rigid bone, the muscle forces produce a rotation of the radius about its rotation center $\mathbf{c}$ at the humeroradial joint:

$$\mathbf{q}_i = \mathbf{R}\mathbf{p}_i + \mathbf{c}, \tag{2}$$

where $\mathbf{R}$ denote the rotation matrix.

The rotation matrix $\mathbf{R}$ can be computed by adapting Arun's algorithm for rigid transformation as follows:

1. Step 1: Move the points so that the rotation center $\mathbf{c}$ coincides with the origin of the world coordinate system:
$$\mathbf{r}_i = \mathbf{p}_i - \mathbf{c}, \quad \mathbf{r}'_i = \mathbf{q}_i - \mathbf{c}. \tag{3}$$

2. Step 2: Compute the rotation matrix as follows. First, compute matrix $\mathbf{M}$ from the sum of outer product:

$$\mathbf{M} = \sum_i \mathbf{r}'_i \mathbf{r}_i^\top. \tag{4}$$

Next, perform singular value decomposition (SVD) on $\mathbf{M}$:

$$\mathbf{M} = \mathbf{U}\Sigma\mathbf{V}^\top. \tag{5}$$

Then, the rotation matrix $\mathbf{R}$ is given by

$$\mathbf{R} = \mathbf{U}\mathbf{V}^\top. \tag{6}$$

As $\mathbf{U}$ and $\mathbf{V}$ are both orthogonal matrices, the matrix $\mathbf{R}$ obtained by Eq. 6 is also an orthogonal matrix, as required for a rotation matrix. Note that $\mathbf{R}$ denotes rotation about the origin of the world coordinate system. Due to Step 1, $\mathbf{R}$ is effectively a rotation about the rotation center $\mathbf{c}$.

3. Step 3: Rotate all points $\mathbf{p}_j$ on the radius and the hand bones about the fixed rotation center $\mathbf{c}$:

$$\mathbf{q}_j = \mathbf{R}\mathbf{p}_j + \mathbf{c}. \tag{7}$$

Now, the radius rotation algorithm can be summarized as follows:

Radius Rotation

```
Initialize forearm model at initial pose.
for each time step over the range of forearm rotation do
    Obtain tangential force vectors f_i for each i.
    Compute target positions q_i for each i (Eq. 1).
    Compute rotation matrix using modified Arun's algorithm.
    Apply rotation on radius and hand bones (Eq. 7).
```

4.3.2 Experimental Procedure

Two implementations of this model were tested:

(a) Force vectors with equal magnitudes, without DRUJ force

This is the simplest method because there is no need to estimate the relative strength of the forces. In particular, the PT vectors and S vectors have small equal magnitudes, and the DRUJ vectors have zero magnitude.

(b) Force vectors with unequal magnitudes, with DRUJ force

In this case, the magnitudes of the force vectors are empirically set to produce radius motion that is as close to the desired motion as possible. Obviously, this method is neither ideal nor useful for subject-specific modeling. Nevertheless, it helps to illustrate that appropriate muscle forces, along with the DRUJ constraint, can produce the desired forearm motion. This model can potentially be generalized to Version 4, which eliminates the empirical setting of force magnitudes.

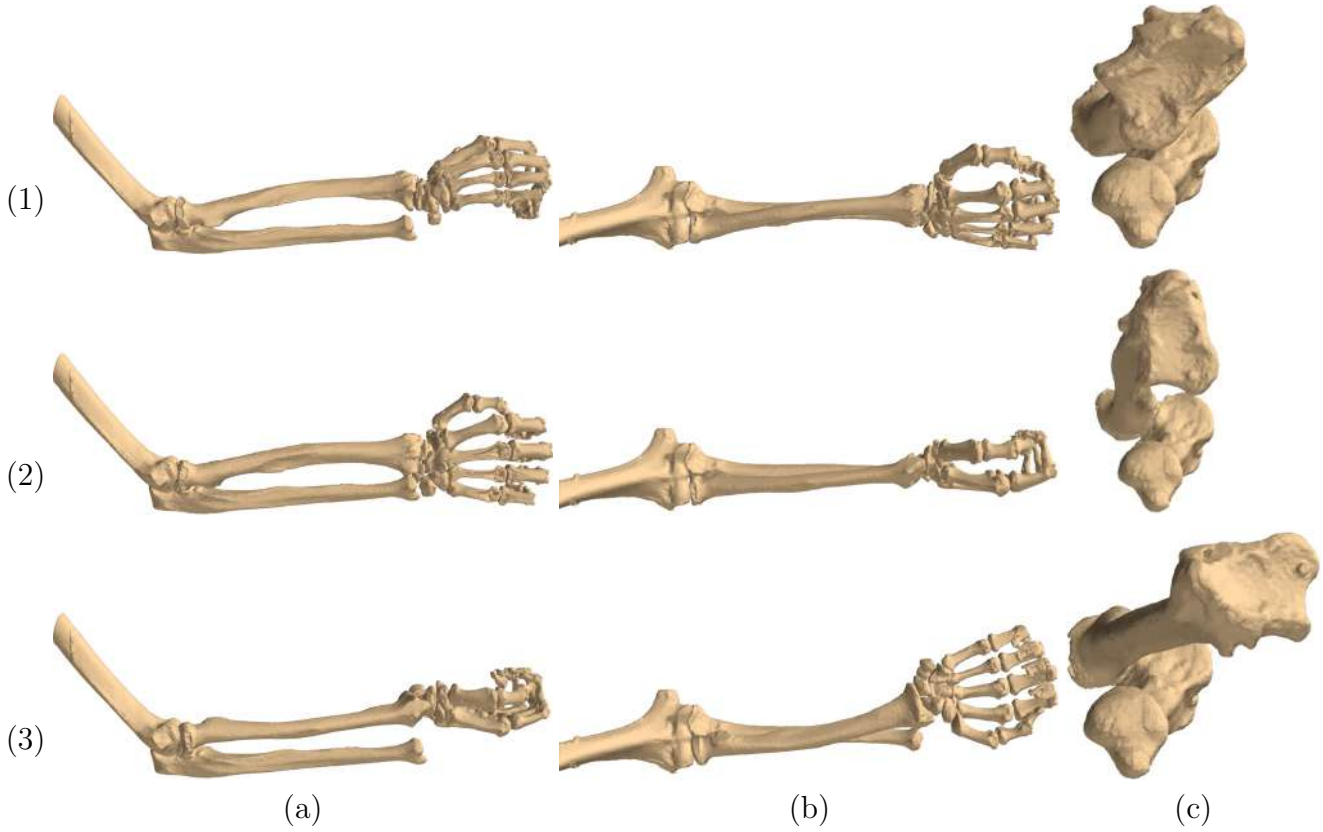

Figure 25: Results of Version 2(a). (1) Full pronation. (2) Approximate neutral pose. (3) Full supination. (a) Side view. (b) Top-down view. (c) Frontal view without humerus and hand bones.

4.3.3 Results and Discussions

For Version 2(a), the radius rotates about the ulna with bone collision detected (Fig. 25). The hand rotates with the radius as a single rigid object. At the elbow joint, there is bone collision. At the wrist joint, the gap between the radius and the ulna is not properly maintained, as the distal radius noticeably breaks away from the ulnar head during supination. Since both the elbow joint and wrist joint constraints are not satisfied, this implementation yields incorrect results.

The results for Version 2(a) show that there is too much superior-inferior (up-down) motion and too little mediolateral (sideway) and axial motion. The desired motion of the radius is not produced. Since the DRUJ constraint is not enforced, it is expected that the net effects of muscles alone are not sufficient to yield the desired motion of the radius.

For Version 2(b), the radius rotates about the ulna, and the hand rotates with the radius as a single rigid object. At the elbow joint, there is also a slight amount of bone collision. At the wrist joint, there is a small amount of bone collision, and the gap between the radius and the ulna is only partially maintained. Unlike in Version 1, the distal radius no longer breaks away from the distal ulna, because the DRUJ constraint is now enforced.

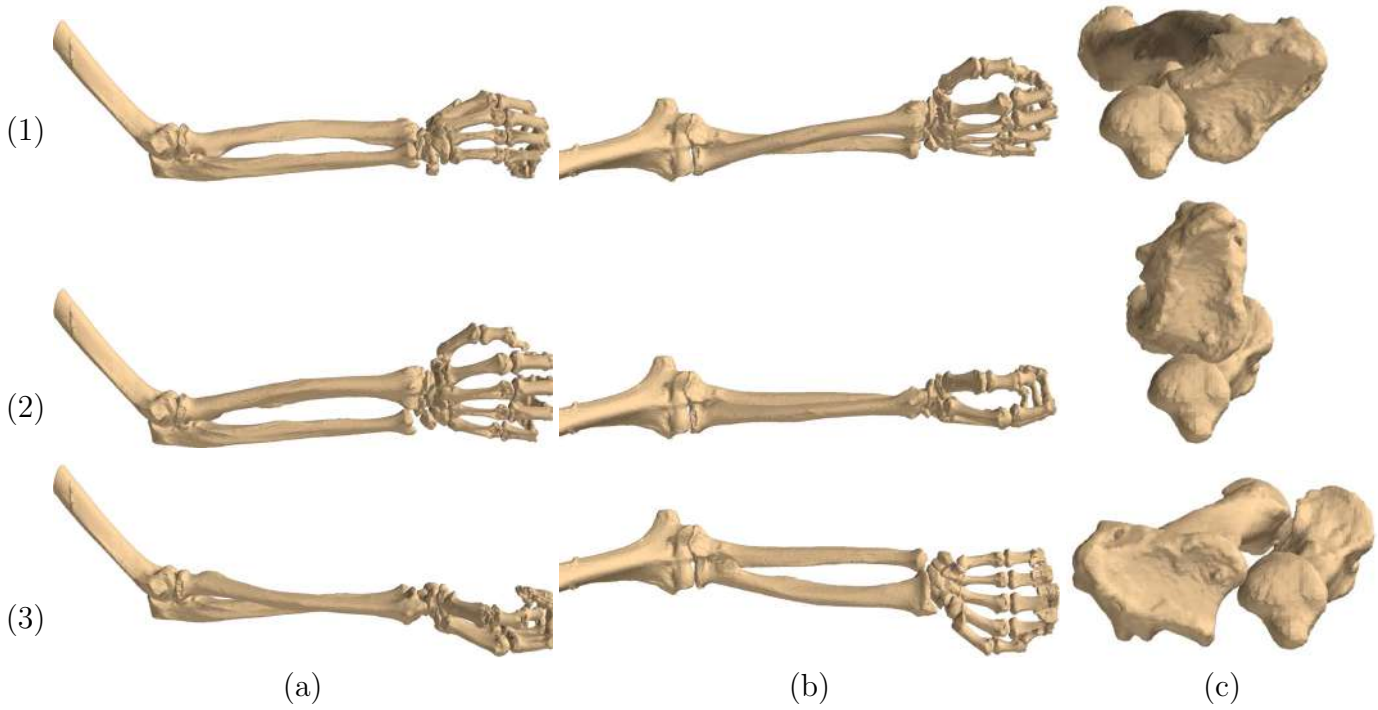

Figure 26: Results of Version 2(b). (1) Full pronation. (2) Neutral pose. (3) Full supination. (a) Side view. (b) Top-down view. (c) Frontal view without humerus and hand bones.

The result of Version 2(b) is more reasonable than that of Version 2(a), as the desired motion of the radius is more or less maintained. Nevertheless, in Version 2(b), the radius still does not have enough axial rotation. In summary, Versions 1 and 2(b) provide simple approximations that can be generalized to Versions 3 and 4. In particular, Version 4 is a subject-specific physiological model that generates the most accurate forearm rotation.

5 Conclusions

This QE paper presents initial findings on computational modeling of forearm rotation. Existing models of forearm rotation include static models, kinematic models and dynamic models. They either require multiple CT scans or are too sophisticated and cumbersome for routine clinical applications. The models in this QE paper are developed to address these issues. Given a single CT scan of the forearm, the proposed models can generate 3D motion for the radius, with the ulna remaining stationary.

Two versions of forearm rotation modeling are proposed. Version 1 is the simplest version and is entirely based on geometrical considerations. In this version, the ulna is stationary, and the radius rotates with the hand bones about a fixed rotation axis. Experimental results show that this version does not produce accurate forearm rotation.

Version 2 is a quasi-physiological model of radius motion, implemented by emulating the net effects of the pronator and supinator muscles. For simplicity, the ulna remains stationary.

Two implementations of Version 2 are proposed, namely 2(a) and 2(b). Version 2(a) sets the force vectors to have small equal magnitudes and the DRUJ vectors to have zero magnitude. This version yields incorrect results.

Version 2(b) is implemented by empirically setting the force vectors to produce radius motion that is as close to the desired motion as possible. This version is neither ideal nor useful for subject-specific modeling. Nevertheless, it shows that the appropriate muscle forces, along with the DRUJ constraint, can yield desired forearm motion. This version can potentially be generalized to the physiological model of Version 4.

The plan for future work is to generalize the models to Version 3 and eventually Version 4 that incorporates ulna motion and constraints due to DRUJ, PRUJ, HRJ, HUJ, ligaments and IOM. In addition, model validation will be performed in collaboration with surgeons at Singapore General Hospital.

6 Acknowledgement

The author would like to thank Dr. Howe Tet Sen and his surgical team from Singapore General Hospital for their support and collaboration.

References

[1] George D Chloros et al. "Reconstruction of Essex-Lopresti injury of the forearm". In: *The Journal of hand surgery* 33.1 (2008), pp. 124–130.

[2] Bryan J Loeffler, Jennifer B Green, and David S Zelouf. "Forearm instability". In: *The Journal of hand surgery* 39.1 (2014), pp. 156–167.

[3] Marlis T Sabo and Adam C Watts. "Longitudinal instability of the forearm: anatomy, biomechanics, and treatment considerations". In: *Shoulder & Elbow* 4.2 (2012), pp. 119–126.

[4] Hisao Moritomo et al. "Interosseous membrane of the forearm: length change of ligaments during forearm rotation". In: *The Journal of hand surgery* 34.4 (2009), pp. 685–691.

[5] Takuya Kiyokawa et al. "Estimation of kinematics parameters dependent on pronation supination for modeling forearm skeletal system based on CT images". In: *2015 IEEE/SICE International Symposium on System Integration (SII)*. IEEE. 2015, pp. 422–427.

[6] G Elisabeta Marai et al. "Estimating joint contact areas and ligament lengths from bone kinematics and surfaces". In: *IEEE Transactions on Biomedical Engineering* 51.5 (2004), pp. 790–799.

[7] P Furnstahl et al. "A morphological approach to the simulation of forearm motion". In: *2009 Annual International Conference of the IEEE Engineering in Medicine and Biology Society*. IEEE. 2009, pp. 7168–7171.

[8] Jean-Pierre Baeyens et al. “In vivo 3D arthrokinematics of the proximal and distal radioulnar joints during active pronation and supination”. In: *Clinical Biomechanics* 21 (2006), S9–S12.

[9] Joseph J Crisco et al. “Effects of distal radius malunion on distal radioulnar joint mechanics—an in vivo study”. In: *Journal of Orthopaedic Research* 25.4 (2007), pp. 547–555.

[10] Shian Chao Tay et al. “In-vivo kinematic analysis of forearm rotation using helical axis analysis”. In: *Clinical Biomechanics* 25.7 (2010), pp. 655–659.

[11] Douglas C Moore et al. “Three-dimensional in vivo kinematics of the distal radioulnar joint in malunited distal radius fractures”. In: *The Journal of hand surgery* 27.2 (2002), pp. 233–242.

[12] Shingo Abe et al. “Three-Dimensional In Vivo Analysis of Malunited Distal Radius Fractures With Restricted Forearm Rotation”. In: *Journal of Orthopaedic Research®* 37.9 (2019), pp. 1881–1891.

[13] Shian Chao Tay et al. “A method for in-vivo kinematic analysis of the forearm”. In: *Journal of biomechanics* 41.1 (2008), pp. 56–62.

[14] Junichi Miyake et al. “In vivo three-dimensional motion analysis of chronic radial head dislocations”. In: *Clinical Orthopaedics and Related Research®* 470.10 (2012), pp. 2746–2755.

[15] Fabien Péan et al. “Physical simulation of the interosseous ligaments during forearm rotation”. In: *CAOS* 1 (2017), pp. 181–188.

[16] Seung-Han Shin et al. “Is the Fovea Ulnaris Truly Isometric during Forearm Rotation?—An In Vivo Retrospective Analysis Using Superimpositions of Three-Dimensional Reconstructions”. In: *Applied Sciences* 12.6 (2022), p. 3108.

[17] Shinsuke Omori et al. “In vivo three-dimensional elbow biomechanics during forearm rotation”. In: *Journal of Shoulder and Elbow Surgery* 25.1 (2016), pp. 112–119.

[18] Kristin Zhao et al. “A technique for quantifying wrist motion using four-dimensional computed tomography: approach and validation”. In: *Journal of biomechanical engineering* 137.7 (2015).

[19] Satoshi Oki et al. “The relationship between the morphological axis and the kinematic axis of the proximal radius”. In: *Surgical and Radiologic Anatomy* 41.4 (2019), pp. 423–429.

[20] Ko Ayusawa, Yosuke Ikegami, and Yoshihiko Nakamura. “Simultaneous global inverse kinematics and geometric parameter identification of human skeletal model from motion capture data”. In: *Mechanism and Machine Theory* 74 (2014), pp. 274–284.

[21] Andreas Aristidou and Joan Lasenby. “Motion capture with constrained inverse kinematics for real-time hand tracking”. In: *2010 4th International Symposium on Communications, Control and Signal Processing (ISCCSP)*. IEEE. 2010, pp. 1–5.

[22] Wei Wang et al. “Comparison of modelling and tracking methods for analysing elbow and forearm kinematics”. In: *Proceedings of the Institution of Mechanical Engineers, Part H: Journal of Engineering in Medicine* 233.11 (2019), pp. 1113–1121.

[23] Maria Laitenberger et al. "Refinement of the upper limb joint kinematics and dynamics using a subject-specific closed-loop forearm model". In: *Multibody System Dynamics* 33.4 (2015), pp. 413–438.

[24] Bart Carelsen et al. "Detection of in vivo dynamic 3-D motion patterns in the wrist joint". In: *IEEE Transactions on Biomedical Engineering* 56.4 (2008), pp. 1236–1244.

[25] Kexiang Li et al. "Estimation of continuous elbow joint movement based on human physiological structure". In: *Biomedical engineering online* 18.1 (2019), pp. 1–15.

[26] James WL Pau, Shane SQ Xie, and Andrew J Pullan. "Neuromuscular interfacing: Establishing an EMG-driven model for the human elbow joint". In: *IEEE Transactions on biomedical engineering* 59.9 (2012), pp. 2586–2593.

[27] Yongsheng Gao et al. "An elbow-biomechanical modeling based on sEMG". In: *Proceeding of the 11th World Congress on Intelligent Control and Automation*. IEEE. 2014, pp. 5238–5243.

[28] Li Le et al. "Using In vivo subject-specific musculotendon parameters to investigate control strategy changes after stroke: An EMG-driven model of elbow joint". In: *Proceedings of the 31st Chinese Control Conference*. IEEE. 2012, pp. 4525–4528.

[29] Yasuharu Koike and Mitsuo Kawato. "Estimation of dynamic joint torques and trajectory formation from surface electromyography signals using a neural network model". In: *Biological cybernetics* 73.4 (1995), pp. 291–300.

[30] Arefeh Pasdar et al. "A comparison between computed muscle control method and static optimization technique to determine muscle forces during a weight training exercise with a dumbbell". In: *2012 19th Iranian Conference of Biomedical Engineering (ICBME)*. IEEE. 2012, pp. 85–90.

[31] Bernard F Morrey, Joaquin Sanchez Sotelo, and Mark E Morrey. *Morrey's The Elbow and Its Disorders E-Book*. Elsevier Health Sciences, 2017.

[32] Emmannuel J. Camus, Fabian Moungondo, and Luc Van Overstraeten. "Chapter 17 - Biomechanics of wrist and elbow". In: *Human Orthopaedic Biomechanics*. Ed. by Bernardo Innocenti and Fabio Galbusera. Academic Press, 2022, pp. 325–338. ISBN: 978-0-12-824481-4. DOI: https://doi.org/10.1016/B978-0-12-824481-4.00037-8. URL: https://www.sciencedirect.com/science/article/pii/B9780128244814000378.

[33] Hisao Moritomo. "The distal interosseous membrane: current concepts in wrist anatomy and biomechanics". In: *The Journal of hand surgery* 37.7 (2012), pp. 1501–1507.

[34] K.S. Saladin. *ISE Anatomy & Physiology: The Unity of Form and Function*. McGraw-Hill Education, 2020. ISBN: 9781260571295. URL: https://books.google.com.sg/books?id=MtFSzQEACAAJ.

[35] Frank H Netter. *Atlas of human anatomy, Professional Edition E-Book: including NetterReference. com Access with full downloadable image Bank*. Elsevier health sciences, 2014.

[36] *MRI Anatomy and Positioning Series Module 1: Upper Extremity Orthopedic Imaging*. URL: https://hca.fujifilm.com/self-learning-activity/docs/UpperExtremityModule/.

[37] Joseph Hamill and Kathleen M Knutzen. *Biomechanical basis of human movement*. Lippincott Williams & Wilkins, 2006.

[38] Saif Ul Islam et al. "The anatomy and biomechanics of the elbow". In: *The Open Orthopaedics Journal* 14.1 (2020).

[39] Thomas W Wright. "Interosseous membrane of the forearm". In: *Journal of the American Society for Surgery of the Hand* 1.2 (2001), pp. 123–134.

[40] Kazuo Noda et al. "Interosseous membrane of the forearm: an anatomical study of ligament attachment locations". In: *The Journal of hand surgery* 34.3 (2009), pp. 415–422.

[41] Hiroshi Watanabe et al. "Contribution of the interosseous membrane to distal radioulnar joint constraint". In: *The Journal of hand surgery* 30.6 (2005), pp. 1164–1171.

[42] Adalbert Kapandji. "Biomechanics of pronation and supination of the forearm." In: *Hand clinics* 17.1 (2001), pp. 111–22.

[43] Jason T Little et al. "Pediatric distal forearm and wrist injury: an imaging review". In: *Radiographics* 34.2 (2014), pp. 472–490.

[44] Anne M Hollister, Harris Gellman, and Robert L Waters. "The relationship of the interosseous membrane to the axis of rotation of the forearm." In: *Clinical Orthopaedics and Related Research* 298 (1994), pp. 272–276.

[45] Kei O Matsuki et al. "In vivo 3D kinematics of normal forearms: analysis of dynamic forearm rotation". In: *Clinical biomechanics* 25.10 (2010), pp. 979–983.

[46] Vivien C Lees. "The functional anatomy of forearm rotation". In: *Journal of hand and microsurgery* 1.02 (2009), pp. 92–99.

[47] P Kasten et al. "Kinematics of the ulna during pronation and supination in a cadaver study: implications for elbow arthroplasty". In: *Clinical Biomechanics* 19.1 (2004), pp. 31–35.

[48] Andrew A. Amis. "Chapter 3 - Biomechanics of the Elbow". In: *Operative Elbow Surgery*. Ed. by David Stanley and Ian A. Trail. Edinburgh: Churchill Livingstone, 2012, pp. 29–44. ISBN: 978-0-7020-3099-4. DOI: https://doi.org/10.1016/B978-0-7020-3099-4.00003-5. URL: https://www.sciencedirect.com/science/article/pii/B9780702030994000035.

[49] Pere Ibáñez-Gimeno et al. "Biomechanics of forearm rotation: force and efficiency of pronator teres". In: *PLoS One* 9.2 (2014), e90319.

[50] Michael Sauerbier and Frank Unglaub. "CHAPTER 27 - Anatomy and Biomechanics of Forearm Rotation". In: *Fractures and Injuries of the Distal Radius and Carpus*. Ed. by David J. Slutsky and A. Lee Osterman. Philadelphia: W.B. Saunders, 2009, pp. 285–296. ISBN: 978-1-4160-4083-5. DOI: https://doi.org/10.1016/B978-1-4160-4083-5.00029-9. URL: https://www.sciencedirect.com/science/article/pii/B9781416040835000299.

[51] BA Barton and EJ Evans. "Movements of the elbow and shoulder during pronation of the forearm". In: *Clinical Anatomy: The Official Journal of the American Association of Clinical Anatomists and the British Association of Clinical Anatomists* 4.6 (1991), pp. 421–432.

[52] Robicheaux G W et al. "Axial Migration of the Radius through a Full Arc of Elbow Flexion/Extension and Forearm Supination/Pronation". In: *ORS 2012 Annual Meeting*. 2012. URL: http://www.ors.org/Transactions/58/2232.pdf.

[53] Brent A Lanting. "The Development and Application of a Forearm Simulator to Investigate Radial Head Biomechanics". In: (2014).

[54] RJ Quigley, GW Robicheaux, and TQ Lee. "The proximal and distal position of the radius relative to the ulna through a full range of elbow flexion and forearm rotation". In: *Journal of Hand Surgery (European Volume)* 39.5 (2014), pp. 535–540.

[55] Takashi Kitamura et al. "The biomechanical effect of the distal interosseous membrane on distal radioulnar joint stability: a preliminary anatomic study". In: *The Journal of hand surgery* 36.10 (2011), pp. 1626–1630.

[56] Hyo-Jin Kim et al. "Influence of forearm rotation on proximal radioulnar joint congruency and translational motion using computed tomography and computer-aided design technologies". In: *The Journal of hand surgery* 36.5 (2011), pp. 811–815.

[57] Karol Galik et al. "The effect of the annular ligament on kinematics of the radial head". In: *The Journal of hand surgery* 32.8 (2007), pp. 1218–1224.

[58] E Sayit et al. "Ulnar variance according to gender and side during aging: An analysis of 600 wrists". In: *Orthopaedics & Traumatology: Surgery & Research* 104.6 (2018), pp. 865–869.

[59] George L Yeh et al. "Effects of forearm rotation on the clinical evaluation of ulnar variance". In: *The Journal of hand surgery* 26.6 (2001), pp. 1042–1046.

[60] JM Jung et al. "Changes in ulnar variance in relation to forearm rotation and grip". In: *The Journal of Bone and Joint Surgery. British volume* 83.7 (2001), pp. 1029–1033.

[61] Toshiyasu Nakamura et al. "Three-dimensional magnetic resonance imaging of the interosseous membrane of forearm: a new method using fuzzy reasoning". In: *Magnetic resonance imaging* 17.3 (1999), pp. 463–470.

[62] T Nakamura, Y Yabe, and Y Horiuchi. "In vivo MR studies of dynamic changes in the interosseous membrane of the forearm during rotation". In: *Journal of Hand Surgery* 24.2 (1999), pp. 245–248.

[63] T Nakamura et al. "In vivo motion analysis of forearm rotation utilizing magnetic resonance imaging". In: *Clinical biomechanics* 14.5 (1999), pp. 315–320.

[64] Erica Kholinne et al. "The role of the interosseous ligament in forearm rotation: A biomechanical study". In: *Journal of Orthopaedic Surgery* 28.3 (2020), p. 2309499020973481.

[65] Elaine L Bukowski. "Atlas of amputations and limb deficiencies: surgical, prosthetic, and rehabilitation principles, ed 3". In: *Physical Therapy* 86.4 (2006), pp. 595–596.

[66] Fabio Carrillo et al. “Digitalization of the IOM: A comprehensive cadaveric study for obtaining three-dimensional models and morphological properties of the forearm’s interosseous membrane”. In: *Scientific reports* 10.1 (2020), pp. 1–15.

[67] Aaron Sodickson et al. “Recurrent CT, cumulative radiation exposure, and associated radiation-induced cancer risks from CT of adults”. In: *Radiology* 251.1 (2009), pp. 175–184.

[68] Mohsen Akbari-Shandiz et al. “MRI vs CT-based 2D-3D auto-registration accuracy for quantifying shoulder motion using biplane video-radiography”. In: *Journal of biomechanics* 82 (2019), pp. 375–380.

[69] Shingo Abe et al. “Analysis of forearm rotational motion using biplane fluoroscopic intensity-based 2D–3D matching”. In: *Journal of biomechanics* 89 (2019), pp. 128–133.

[70] M Foumani et al. “In-vivo three-dimensional carpal bone kinematics during flexion–extension and radio–ulnar deviation of the wrist: Dynamic motion versus step-wise static wrist positions”. In: *Journal of biomechanics* 42.16 (2009), pp. 2664–2671.

[71] Keisuke Matsuki et al. “Three-dimensional measurement of proximal radioulnar space during active forearm pronation”. In: *Journal of Biomechanics* 113 (2020), p. 110120.

[72] Bart Carelsen et al. “4D rotational x-ray imaging of wrist joint dynamic motion”. In: *Medical physics* 32.9 (2005), pp. 2771–2776.

[73] Peng-zhan Chen et al. “Real-time human motion capture driven by a wireless sensor network”. In: *International Journal of Computer Games Technology* 2015 (2015).

[74] Leela D Farr et al. “Anatomy and biomechanics of the forearm interosseous membrane”. In: *The Journal of hand surgery* 40.6 (2015), pp. 1145–1151.

[75] Kunihiro Oka et al. “In vivo three-dimensional motion analysis of the forearm with radioulnar synostosis treated by the kanaya procedure”. In: *Journal of orthopaedic research* 24.5 (2006), pp. 1028–1035.

[76] Lee A Feldkamp, Lloyd C Davis, and James W Kress. “Practical cone-beam algorithm”. In: *Josa a* 1.6 (1984), pp. 612–619.

[77] Wolfgang Wein. “Intensity based rigid 2d-3d registration algorithms for radiation therapy”. In: *Technische Universität München, Diplomarbeit* (2003), pp. 15–27.

[78] Senay Mihcin. “Methodology on Co-Registration of MRI and Optoelectronic Motion Capture Marker Sets: In-Vivo Wrist Case Study”. In: *Hittite Journal of Science and Engineering* 6.2 (2019), pp. 99–107.

[79] Dan Song et al. “Model-based sensorimotor integration for multi-joint control: development of a virtual arm model”. In: *Annals of biomedical engineering* 36.6 (2008), pp. 1033–1048.

[80] F Romero and FJ Alonso. “A comparison among different Hill-type contraction dynamics formulations for muscle force estimation”. In: *Mechanical Sciences* 7.1 (2016), pp. 19–29.

[81] Marcus Blümel et al. "Determining all parameters necessary to build Hill-type muscle models from experiments on single muscles". In: *Biological cybernetics* 106.10 (2012), pp. 543–558.

[82] Chris H. Luebkeman. *What is a Moment?* 1998. URL: https://web.mit.edu/4.441/1_lectures/1_lecture5/1_lecture5.html.

[83] Thomas S Buchanan et al. "Estimation of muscle forces and joint moments using a forward-inverse dynamics model". In: *Medicine and Science in Sports and exercise* 37.11 (2005), p. 1911.

[84] Mamun Bin Ibne Reaz, M Sazzad Hussain, and Faisal Mohd-Yasin. "Techniques of EMG signal analysis: detection, processing, classification and applications". In: *Biological procedures online* 8.1 (2006), pp. 11–35.

[85] Liang Peng et al. "An sEMG-driven musculoskeletal model of shoulder and elbow based on neural networks". In: *2015 Seventh International Conference on Advanced Computational Intelligence (ICACI)*. IEEE. 2015, pp. 366–371.

[86] Jer-Junn Luh et al. "Isokinetic elbow joint torques estimation from surface EMG and joint kinematic data: using an artificial neural network model". In: *Journal of electromyography and kinesiology* 9.3 (1999), pp. 173–183.

[87] Rong Song and Kai-Yu Tong. "Using recurrent artificial neural network model to estimate voluntary elbow torque in dynamic situations". In: *Medical and Biological Engineering and Computing* 43.4 (2005), pp. 473–480.

[88] Darryl G Thelen, Frank C Anderson, and Scott L Delp. "Generating dynamic simulations of movement using computed muscle control". In: *Journal of biomechanics* 36.3 (2003), pp. 321–328.

[89] Munsur Rahman et al. "Musculoskeletal model development of the elbow joint with an experimental evaluation". In: *Bioengineering* 5.2 (2018), p. 31.

[90] Mohsen Sharifi Renani et al. "Calibrating multibody ulno-humeral joint cartilage using a validated finite element model". In: *Multibody System Dynamics* 44.1 (2018), pp. 81–91.

[91] Mohsen Sharifi Renani et al. "Ulna-humerus contact mechanics: Finite element analysis and experimental measurements using a tactile pressure sensor". In: *Medical engineering & physics* 50 (2017), pp. 22–28.

[92] Bane Sullivan and Alexander Kaszynski. "PyVista: 3D plotting and mesh analysis through a streamlined interface for the Visualization Toolkit (VTK)". In: *Journal of Open Source Software* 4.37 (May 2019), p. 1450. DOI: 10.21105/joss.01450. URL: https://doi.org/10.21105/joss.01450.